UNIVERSITÄT
BERN

Thesis Title

Inauguraldissertation
der Philosophisch-naturwissenschaftlichen Fakultät
der Universität Bern

vorgelegt von

Raphael Wolfisberg

von Neuenkirch, LU

Leiter der Arbeit

Prof. Dr. Christoph Kempf
and
Dr. Carlos Ros

Departement für Chemie und Biochemie

Erklärung

gemäss Art. 28 Abs. 2 RSL 05

Name/Vorname: .....

Matrikelnummer: .....

Studiengang: ……

Bachelor ☐ Master ☐ Dissertation ☐

Titel der Arbeit: .....

.....

.....

LeiterIn der Arbeit: .....

.....

Ich erkläre hiermit, dass ich diese Arbeit selbständig verfasst und keine anderen als die angegebenen Quellen benutzt habe. Alle Stellen, die wörtlich oder sinngemäss aus Quellen entnommen wurden, habe ich als solche gekennzeichnet. Mir ist bekannt, dass andernfalls der Senat gemäss Artikel 36 Absatz 1 Buchstabe r des Gesetztes vom 5. September 1996 über die Universität zum Entzug des auf Grund dieser Arbeit verliehenen Titels berechtigt ist.

Ich gewähre hiermit Einsicht in diese Arbeit.

.....
Ort/Datum

.....
Unterschrift

The Thesis Abstract is written here (and usually kept to just this page). The page is kept centered vertically so can expand into the blank space above the title too...

Nomenclature

AAV	Adeno-associated virus
AMDV	Aleutian mink disease virus
B19V	Human parvovirus B19
Bp	Base pair
BPV	Bovine parvovirus
CPV	Canine parvovirus
Da	Dalton
DMEM	Dulbecco modified Eagle's medium
DNA	Deoxyribonucleic acid
dsDNA	Double stranded DNA
EPC	Erythroid progenitor cell
FCS	Fetal calf serum
FPV	Feline parvovirus
GFAV	Gray fox amdovirus
GmDNV	Galleria mellonella densovirus
IF	Immunofluorescence
IP	Immunoprecipitation
ITR	Inverted terminal repeat
Kb	Kilo base
kDa	Kilodalton
mAb	Monoclonal antibody
MVM	Minute virus of mice
MVMi	Immunosuppressive strain of MVM
MVMp	Prototype strain of MVM
Nt	Nucleotide
PCR	Polymerase chain reaction
PPV	Porcine parvovirus

PstDNV	Penaeus stylirostris densovirus
qPCR	Quantitative PCR
SN	Supernatant
ssDNA	Single stranded DNA
SV40	Simian vacuolating virus 40 or Simian virus 40

Contents

List of Figures

List of Tables

Part I

Introduction

1 Introduction

1.1 Morphology

Parvoviruses belong to the smallest of isometric viruses. They are devoid of a lipid envelope and their diameters range from 215 Å (Penaeus stylirostris densovirus, PstDNV) to 255 Å (CPV). The icosahedral nature of parvoviruses was shown unambiguously by X-ray crystallography. The capsid surface of some, particularly invertebrate, parvoviruses appears to be smooth (Galleria mellonella densovirus, GmDNV) whereas others (Adeno-associated virus-2, AAV-2) are spiky at the 3- or 5-fold symmetry axes [1, 2].

1.2 Physicochemical properties

about 75 % protein and 25 % DNA, Mr about 5.5 - 6.2 x 10^6, infectious virion buoyant density is 1.39 - 1.43 gcm^{-3}, in CsCl,mature virions are stable in the presence of lipid solvents, on exposure to pH 3-9 and for most species incubation at 56 ℃ for 60 min, inactivation occurs by treatment with formalin, β-propiolacetone, hydroxylamine, ultraviolet light, and oxidizing agentssuch as sodium hypochlorite

1.3 Taxonomy

The classification of the *Parvoviridae* family is based on morpholological and functional characteristics. Parvoviruses are common animal and insect pathogens that belong to the smallest DNA-containing viruses. Hence the prefix "parvum" which means small in Latin. The name "parvovirus" was first introduced to the literature by Carlos Brailovsky in 1966 [3]. The *Parvoviridae* family comprises all non-enveloped, isometric, small DNA viruses that contain linear single-stranded genomes. Indeed, parvoviruses are the only viruses in the known biosphere that have both single-stranded and linear DNA genomes. The encapsidated single genomic molecule is 4-6 kb in length and terminates in palin-

dromic duplex hairpin telomers. As a consequence of such a simple genome, parvoviruses are highly dependent on their host for diverse functions in their reproduction [1, 4]. The terminal hairpins are fundamental for the unique replication strategy of the *Parvoviridae* family and hence serve as an invariant hallmark for classification. Members of the family *Parvoviridae* infect a wide variety of hosts, ranging from insects to primates. Depending on this feature, the *Parvoviridae* are subdivided into *Parvovirinae* infecting vertebrates and *Densovirinae* infecting insects and other arthropods, respectively. The *Parvovirinae* subfamily is further subdivided into eight genera: *Amdoparvovirus*, *Aveparvovirus*, *Bocaparvovirus*, *Copiparvovirus*, *Dependoparvovirus*, *Erythroparvovirus*, *Protoparvovirus* and *Tetraparvovirus*. The subdivision into the eight genera is based on differences in transcription maps, organization of the ITRs, the ability to replicate efficiently either autonomously or with helper virus and sequence homology amongst the *Parvovirinae* subfamily [5, 2].

1.3.1 The *parvovirinae* subfamily

Amdoparvovirus

The genus *Amdoparvovirus* shares most characteristics with the genera *Bocaparvovirus* and *Protoarvovirus*. Mature virions exclusively contain negative strand genomic DNA of approximately 4.8 kb in length harbouring dissimilar palindromic sequences at each end [6, 7]. Only two distant species have been reported. Firstly, *Carnivore amdoparvovirus 1*, which comprises only Aleutian mink disease virus (AMDV) and secondly, *Carnivore amdoparvovirus 2*, which encompasses solely gray fox amdovirus (GFAV) [8]. Permissive replication is tightly restricted to Crandell feline kidney cells. In contrast to the members of the genera *Bocaparvovirus* and *Protoparvovirus*, the virion surface displays three mounds elevated around the threefold icosahedral axis of symmetry. However, several structure features were ascertained to be similar to those found in B19V, CPV, FPV and MVM. Such appearance is comparable to those observed for the genus *Dependoparvovirus* [9]. Remarkably, there is no evidence of a phospholipase 2A enzymatic core within the naturally truncated N-VP1 terminus of members belonging to the genus *Amdoparvovirus* as it is common to the other genera of the subfamily *Parvovirinae* [2].

Aveparvovirus

Copiparvovirus

Bocaparvovirus

The name of the genus is derived from bovine and canine, referring to the two hosts of the first identified members of this genus. The genomes of members of the genus *Bocaparvovirus* are quite distinct from all other viruses in the subfamily *Parvovirinae*. As the members of the genera *Protoparvovirus* and *Amdoparvovirus* they contain non-identical imperfect palindromic sequences at both ends of their 5.5 kb genome. Mature virions contain mainly, but not exclusively, negative strand ssDNA [10, 11]. All RNA transcripts are generated from a single promoter at map unit 4.5. BPV RNA transcripts are alternatively spliced and polyadenylated either at an internal site or at the 3'-end of the genome. Noteworthy, bovine parvovirus (BPV), the main representative, encodes a 22.5 kDa nuclear phosphoprotein, NP-1, whose function still remains unknown. This protein is distinct from any other parvovirus-encoded polypeptide [12].

Dependoparvovirus

Positive and negative strand ssDNA is distributed indifferently among mature virions belonging to the genus *Dependoparvovirus* [13, 14]. The 4.7 kb DNA molecule contains identical ITRs of 145 nt, the first 125 nt of which form a palindromic sequence [15]. Three mRNA promoters that are located at map units 5, 19 and 40 initiate transcription that can be terminated in two polyadenylation sites located at the right-hand end or alternatively, in the middle of the genome [16, 17]. Common for all currently accepted replication-defective members of the genus *Dependoparvovirus* is their strict dependence upon helper adenoviruses or herpesviruses [18, 19, 20]. Therefore, their host range tropism strongly depends on the one of the helper virus. The only exceptions are the autonomously replicating duck and goose parvoviruses which are also comprised within the *Dependoparvovirus* genus based on phylogenetic analysis [2]. The most important members of this genus are the adeno-associated viruses (AAV). They attracted considerable interests since at least one of them, AAV-2, has been reported to integrate site-specifically into human chromosome 19 [21, 22, 23, 24]. This characteristic makes AAV a promising candidate for creating viral vectros for gene therapy. As a well characterized member of the *Dependoparvoviruses* AAV-2 represents the model virus among

this genus.

Erythroparvovirus

Equivalent numbers of positive and negative sense ssDNA are packaged into infectious virions of the genus *Erythroparvovirus*. As in the case with the genus *Dependoparvovirus*, the 5.5 kb ssDNA molecule contains identical ITRs of 383 nt in length at both the 3' and the 5' end. The first 365 nt of those secondary elements form palindromic sequences [25]. Transcription is regulated by a single mRNA promoter located at map unit 6 [26]. A distal polyadenylation site for use in termination of RNA synthesis is located at the far right side. Additionally, transcripts may be terminated at an unusual internal polyadanylation site in the middle of the genome [27]. Viruses belonging to this genus are highly erythrotropic, meaning that efficient replication only occurs in rapidly dividing erythroid progenitor cells (EPCs) such as erythroblasts and megakaryocytes present in the bone marrow. B19V, a human pathogen that causes fifth disease, polyarthropathia, anemic crises in children with underlying hematological diseases (e.g. sickle cell anemia or thalassemia) and intrauterine infections (with hydrops fetalis in some cases) [28] represents the model virus among the genus *Erythroparvovirus*.

Protoparvovirus

Protoparvoviruses were the first members of the subfamily *Parvovirinae* to be discovered in 1959 [29]. Some members of the genus contain positive strand DNA in variable proportions up to 50 % [30]. In mature virions of other members, virtually only negative strand DNA occurs. What they have in common are their hairpin structures at both the 5' and 3' ends of the linear 5 kb ssDNA molecule that differ in both sequence and predicted structure [31]. Transcription of the genome is regulated by two mRNA promoters at map units 4 and 39 [32]. There is only one polyadenylation site at the 3' end. Viral replication provokes characteristic cytopathic effects in cell culture. Many species display hemagglutination with erythrocytes of one or several species. The genus *Protoparvovirus* is primarily represented by MVM [2, 4].

Tetraparvovirus

Genus	Species	Virus or virus variants
Amdoparvovirus	***Carnivore amdoparvovirus 1***	Aleutian mink disease virus
	Carnivore amdoparvovirus 2	Gray fox amdovirus
Aveparvovirus	***Galliform aveparvovirus 1***	Chicken parvovirus
		Turkey parvovirus
Bocaparvovirus	*Carnivore bocaparvovirus 1*	Canine minute virus
	Carnivore bocaparvovirus 2	Canine bocavirus 1
	Carnivore bocaparvovirus 3	Feline bocavirus
	Pinniped bocaparvovirus 1	California sea lion bocavirus
		California sea lion bocavirus
	Pinniped bocaparvovirus 2	California sea lion bocavirus
	Primate bocaparvovirus 1	Human bocavirus 1
		Human bocavirus 3
		Gorilla bocavirus
	Primate bocaparvovirus 2	Human bocavirus 2a
		Human bocavirus 2b
		Human bocavirus 2c
		Human bocavirus 4
	Ungulate bocaparvovirus 1	Bovine parvovirus
	Ungulate bocaparvovirus 2	Porcine bocavirus 1
		Porcine bocavirus 2
		Porcine bocavirus 6
	Ungulate bocaparvovirus 3	Porcine bocavirus 5
	Ungulate bocaparvovirus 4	Porcine bocavirus 7
	Ungulate bocaparvovirus 5	Porcine bocavirus 3
		Porcine bocavirus 4-1
		Porcine bocavirus 4-2
Copiparvovirus	***Ungulate copiparvovirus 1***	Bovine parvovirus 2
	Ungulate copiparvovirus 2	Porcine parvovirus 4
Dependoparvovirus	***Adeno-associated dependoparvovirus A***	Adeno-associated virus-1
		Adeno-associated virus-2
		Adeno-associated virus-3
		Adeno-associated virus-4

Genus	Species	Virus or virus variants
		Adeno-associated virus-6
		Adeno-associated virus-7
		Adeno-associated virus-8
		Adeno-associated virus-9
		Adeno-associated virus-10
		Adeno-associated virus-11
		Adeno-associated virus-12
		Adeno-associated virus-13
		Adeno-associated virus-S17
	Adeno-associated dependovirus B	Adeno-associated virus-5
		Bovine adeno-associated vi
		Caprine adeno-associated v
	Anseriform dependoparvovirus 1	Duck parvovirus
		Goose parvovirus-PT
		Goose parvovirus
	Avian dependovirus 1	Avian adeno-associated viru
	Chiropteran dependoparvovirus 1	Bat adeno-associated virus
	Pinniped dependoparvovirus 1	California sea lion adeno-as
	Squamate dependoparvovirus 1	Snake adeno-associated vir
Erythroparvovirus	***Primate erythroparvovirus 1***	Human parvovirus B19-Au
		Human parvovirus B19-J35
		Human parvovirus B19-Wi
		Human parvovirus B19-A6
		Human parvovirus B19-Lal
		Human parvovirus B19-V9
		Human parvovirus B19-D9
	Primate erythroparvovirus 2	Simian parvovirus
	Primate erythroparvovirus 3	Rhesus macaque parvovirus
	Primate erythroparvovirus 4	Pig-tailed macaque parvovi
	Rodent erythroparvovirus 1	Chipmunk parvovirus
	Ungulate erythroparvovirus 1	Bovine parvovirus 3
Protoparvovirus	*Carnivore protoparvovirus 1*	Feline parvovirus

Genus	Species	Virus or virus variants
		Canine parvovirus
		Mink enteritis virus
		Racoon parvovirus
	Primate protoparvovirus 1	Bufavirus 1a
		Bufavirus 1b
		Bufavirus 2
	Rodent protoparvovirus 1	H-1 parvovirus
		Kilham rat virus
		LuIII virus
		Minute virus of mice (proto
		Minute virus of mice (immu
		Minute virus of mice (Miss
		Minute virus of mice (Cutt
		Mouse parvovirus 1
		Mouse parvovirus 2
		Mouse parvovirus 3
		Mouse parvovirus 4
		Mouse parvovirus 5
		Hamster parvovirus
		Tumor virus X
		Rat minute virus 1
	Rodent protoparvovirus 2	Rat parvovirus 1
	Ungulate protoparvovirus 1	Porcine parvovirus Kresse
		Porcine parvovirus NADL-2
Tetraparvovirus	*Chiropteran tetraparvovirus 1*	Eidolon Helvum (bat) parv
	Primate tetraparvovirus 1 Human parvovirus 4 G1	PARV4G1
		Human parv4 G2
		Human parv4 G3
		Chipmanzee parv4
	Ungulate tetraparvovirus 1	Bovine hokovirus 1
		Bovine hokovirus 2
	Ungulate tetraparvovirus 2	Porcine hokovirus

Genus	Species	Virus or virus variants
	Ungulate tetraparvovirus 3	Porcine Cn virus
	Ungulate tetraparvovirus 4	Ovine hokovirus

1.4 Tropism

Most parvoviruses, such as MVM, CPV and FPV, show specific host ranges and tissue tropisms. The majority of the parvoviruses are members of those tightly controlled viruses. However, some parvoviruses, as for example many of the AAVs, infect many hosts and a variety of tissues. Understanding controls of these properties for autonomous parvoviruses show great promise for the therapeutic delivery to be controlled or modified in gene therapy applications [33].

To date, two independent strains of the parvovirus MVM have been described to occur in mice. Both strains display disparate *in vitro* tropism and *in vivo* pathogenicity despite differing by only 14 amino acids in their capsid proteins. Fist, MVMp, the prototype strain, was originally isolated from a contaminated murine adenovirus stock and was shown to replicate efficiently in mouse fibroblasts [34]. Secondly, MVMi, the immunosuppressive strain, was recovered from an infected EL-4 T-cell lymphoma culture [35]. Although MVMi infection may result in pathology of infected mice, it has been shown that the infection more likely interferes with numerous T-cell functions *in vitro*. The infection rather causes problems for the ongoing study the mice are being used for as the immune system will be activated, the activity of T-lymphocytes or B-lymphocytes will be altered and tumor formation may be suppressed [36, 37, 38].

As above-mentioned, it has been shown that the allotropic MVM strains, MVMi and MVMp, differ in their target cell tropism. In order to map the viral sequences responsible for that difference, chimeric viral genomes were constructed *in vitro* from infectious genomic clones of both strains. The differences in the cell tropism between MVMi and MVMp have been mapped to the capsid gene, in particular to the VP2 residues 317 and 321. Both residues are located at the base of the threefold spike of the virion and are involved in controlling the cell tropism of the two distinct MVM strains [39, 40, 41]. Interestingly, residue 321 aligns with residue 323 of CPV, that itself is a critical determinant for CPV host range tropism. Further residues (VP2 residues 399, 553 and 558) were identified in MVMi to be able to confer fibrotropism to single site-directed mutants. Those residues cluster around the twofold dimple-like depression [42].

In general, tissue tropism determining amino acids were found be located on, or near, the viral surface, mainly by raised structural elements around the threefold axes of symmetry. Differences in tropism and pathogenicity have also been mapped to the capsid proteins of Aleutian mink disease parvovirus [43], porcine parvovirus (PPV) [44], CPV [45, 46], and FPV [47] in a capsid region analogous to that observed for MVM. Although the same structural element of viruses is involved in mediating host and tissue tropisms, each appears to be affecting a different mechanism. Host ranges of CPV and FPV are controlled by receptor binding, whereas the cell tropisms of MVM appear to be due to restrictions of interactions with intracellular factors [42, 33].

1.5 Structure

1.5.1 Parvoviruses in general

Parvovirus capsids are devoid of a lipid envelope and have an average diameter of 18 to 26 nm. The viral capsid is made up of 60 copies of between two and four structural proteins that overlap each other. For each virus there is one major capsid protein present in the capsid structure. Minor proteins form the same core structure, but differ in the sequence length on their amino termini. The capsid proteins display a T=1 icosahedral symmetry and are variously designated VP1-VP4. Thus, the capsid has a 5-3-2 point group symmetry containing 31 rotational symmetry elements that intersect at the center: six fivefolds, ten threefolds, and fifteen twofolds. Despite the differences in protein forms and the low homology between some of the viruses, several structural elements on the capsid surface are common to most parvoviruses. These include raised cylindrical channels at the fivefold axes surrounded by depressed, canyon-like regions. Further shared surface characteristics are protrusions at the threefold axes, termed as spikes or peaks, and dimple-like depressions at the icosahedral twofold axes. A common feature of parvoviruses is their high resistance to physicochemical treatments. This stability provides an effective protection to the fragile, condensed genome in the extracellular environment ensuring transmission between their hosts. The ssDNA genome consists of approximately 5000 bases, packed as either a positive or, more usually, as a negative sense strand. At the 5' and 3' ends, the genome harbors palindromic sequences of about 120 to 250 nucleotides, that form secondary hairpin structures which are essential for the initiation of viral genome replication [48, 49, 50, 42, 51, 52, 33].

1.5.2 MVM

Both DNA-containing full and empty particles were crystallized in the monoclinic space group C2. Following data processing and refinement, the resulting electron density map was interpreted with respect to the amino acid sequence of MVMi. The known CPV structure was used as a phasing model since 52 % of the 578 amino acids in VP2 of MVM are identical to CPV. The polypeptide chain of the major structural protein, VP2, could be traced from residue 39 to residue 587 at the C-terminus [53]. The common c-terminal part of the structural proteins has an eight-stranded antiparallel β-barrel topology, frequently found in viral capsid proteins [54]. Large loops between the β-strands of the β-barrel that form the principal surface features, particularly the threefold spikes, and determine host-range tropism were found to be quite dissimilar in MVM and CPV. The first 37 amino acids are not visible in the electron density map. Since the N-VP2 terminal part contains a predominantly poly-glycine conserved sequence, it might be highly flexible. There is density extending along the fivefold channels of the MVMi capsid that was modeled as the glycine-rich N-terminal region [55, 56]. *In vitro*, trypsin digestion of full MVM virions results in a truncated VP3 polypeptide that still contains the glycine-rich sequence. In this way, most VP2 N-termini can be cleaved. These findings suggest that there is a dynamic situation at the fivefold channel. In one model, one in five amino termini are externalized along the fivefold axes and are accessible for cleavage. Newly created, cleaved N-VP3 termini could withdraw into the virion and be replaced at the surface by an uncleaved N-VP2 terminus. [57, 42]. A substantial amount of internal electron density could be related to 10 DNA nucleotides that were previously found in the analysis of the structure of CPV [58, 59]. For MVM, 19 additional DNA nucleotides were identified in a difference electron-density map with respect to the data of empty particles. Thus, 29 ordered, or partially ordered, nucleotides per icosahedral asymmetric unit imply that approximately 34 % of the total genome display icosahedral symmetry. This finding, and the conservation of base-binding sites between MVMi and CPV, identifies a DNA-recognition site on the parvoviral capsid interior [42].

1.6 Nucleic Acid

1.6.1 Genome organization

1.6.2 Transcriptome

1.7 Viral proteins

1.7.1 Structural Proteins

1.7.2 Non-structural proteins

1.8

1.8.1

1.8.2

2 Methods

2.1 Cell Cultures

A9 ouab^{r}l1 cells, a derivative from the original HGPRT^{-} L-cell line A9 represent a clone resistant to 10^{-3} M ouabain after nitrosoguanidine mutagenesis [60]. NB324K cells are a clone of SV40-transformed human newborn kidney cells [61]. The SV40 large T antigen was detected by immunofluorescent staining with monoclonal antibodies [62]. However, NB324K cells do not produce infectious SV40 spontaneously. Both cell lines, A9 mouse fibroblasts and NB324K cells, were routinely propagated under a minimal number of passages in DMEM supplemented with 5 % of heat inactivated fetal bovine serum at 37 ℃ in 5 % CO_2 atmosphere.

2.1.1 Freezing and thawing of cells

Before use the A9 mouse fibroblasts or NB324K cells were thawed at 37 ℃ and cultured in 5 mL of pre-warmed DMEM supplemented with 5 % FCS. The medium was replaced every 3 to 4 days. In order to freeze the cells for long storage in liquid nitrogen they were passed the day before, to ensure exponential growth. Subsequently, 7.5 % DMSO was added and the cells were frozen slowly at -70 ℃ over night before transfer to liquid nitrogen.

2.2 Virus Stocks

Stocks of MVM without detectable levels of VP3 were propagated on A9 mouse fibroblast monolayers. As soon as the cytopathic effect became evident, the supernatant was collected and pre-cleared from cell debris by low-speed centrifugation. Thereby, intracellular, VP3 rich capsids were discarded. In order to remove low-molecular contaminants, virus containing SN was pelleted through 20 % sucrose cushion in PBS by

ultra-centrifugation. Virus titers were determined by qPCR as DNA-packaged particles per microliter.

2.2.1 Separation of empty and full capsids

Sucrose purified capsids were prepared as previously described in section 2.2, page 13. The virus pellet was resuspended in 10 mL PBS. Caesium chloride was added to a density of 1.38 g/mL adjusted by refractometry (η=1.371) at 4 ℃. The gradient was centrifuged to equilibrium for 24 h at 41000 rpm and 4 ℃ in a Beckmann SW-41 Ti rotor. Gradients were fractionated and tested for intact capsids by dot blot analysis using B7 mAb. CsCl was depleted from the corresponding fractions by size-exclusion chromatography through PD-10 desalting columns and concentrated by ultra-centrifugation when required.

2.3 Freezing bacteria stocks in glycerol

Bacteria were frozen in dry ice. A volume of 700 μL of the bacteria culture that was grown over night in LB-medium was mixed with 300 μL of 50 % glycerol in a cryotube. In order to mix well the glycerol the cryotube was vortexed intensively. Following snap-freeze in dry ice the bacteria were stored at -70 ℃.

2.4 Anion-exchange chromatography

A Mono Q HR 5/5 (Pharmacia) column (5 x 50 mm) was used to analyse viral samples. The Mono Q column was connected to the ÄKTAmicro chromatography system (GE Healthcare) that was operated by the UNICORN control software. The Mono Q column was equilibrated with six column volumes (CV) starting buffer (20 mM Tris-HCl, 1 mM EDTA, pH 7.2). Samples (1 mL) containing at least 10^{10} virus particles in 10 mM Tris-HCl, 1 mM EDTA, pH 8 were applied to the Mono Q column trough a 2 mL loop. After eluting the protein, which did not bind to the column in the starting buffer, a linear salt gradient (0-2 M NaCl) in 20 mM Trsi-HCl, 1 mM EDTA, pH 7.2, was applied. Fractions of 0.185 mL were collected in 96-well plates. Viral genomes in each fraction were quantified by qPCR. All buffers were filtered and degassed before application to the Mono Q column.

2.5 Quantitative PCR

Amplification of MVM DNA and real-time detection of PCR products were performed by using BioRad CFX96 technology with SYBR green supermix. PCR was carried out by using the hot-start iTaq™ DNA polymerase (Bio-Rad Laboratories) following the manufacturer's guide-lines. Viral DNA was isolated using DNeasy blood and tissue kit. Elution of the purified vDNA was carried out using 100 μL elution buffer. As templates 2 μL of the isolated viral DNA were used for the PCR reaction and were added to the following master mix:

Component	**Amount**	**Final concentration**
dH_2O, PCR grade	6 μL	-
Forward primer, 10 pM	1 μL	0.5 pM
Reverse primer, 10 pM	1 μL	0.5 pM
2x IQ™ SYBR® Green Supermix	10 μL	1x
Total volume	**18 μL**	

Table 2.1: Master mix for quantitative PCR. In order to minimize pipetting errors a master mix was prepared. Following preparation the master mix was distributed across the 96 well plates. The master mix contains all the ingredients which are required for the DNA amplification except the initial DNA template that differs among the samples.

To ensure accurate quantification, the 96-well plates containing master mix and template DNA were shortly spun and transferred into the BioRad CFX96 unit. The following PCR program was used for quantification of viral DNA:

Cycles	**Step**	**Temperature**	**Time**
1x	Initial denaturation	95 ℃	300 s
40x	Denaturation	95 ℃	15 s
	Annealing	61 ℃	15 s
	Extension	72 ℃	15 s
1x	Final denaturation	95 ℃	60 s
1x	Melting curve	65 ℃ up to 95 ℃	0.1 ℃/s

Table 2.2: PCR conditions for the amplification and real-time detection of MVM DNA.

To provide standards for sample quantification, serially diluted plasmids containing the

entire MVM genomic DNA were used. For cell number variations that may exist between the samples, the number of applied cells per PCR reaction needed to be quantified for normalization as well. For this purpose quantification of cellular β-actin gene was performed. After normalization, direct comparison of the results is possible. β-actin quantification was carried out with the same PCR conditions outlined in table 2.2, 15.

2.5.1 Immunoprecipitation

Either *in vitro* treated viruses or viruses from cell extracts were transferred to LoBind tubes that were pre-blocked with PBS containing 1 % bovine serum albumin (PBSA 1 %). The volume was adjusted to 200 μL with PBSA 1 %. The antibody was added in excess and incubated with the viral capsids for 1 h at 4 ℃ on a rotary shaker. Subsequently, 20 μL protein G-agarose beads were added. Following overnight incubation at 4 ℃ and centrifugation at 2500 rpm for 5 min the supernatant was discarded. The beads were washed 4 times with PBSA 1 %. To remove the BSA an additional wash step was carried out with PBS. Finally, the beads were frozen at -20 ℃ until further use or immediately processed.

2.5.2

2.6

2.6.1

2.6.2

Part II

Publication

1 Wolfisberg et al., Journal of Virological Methods, 2013

Impaired genome encapsidation restricts the *in vitro* propagation of human parvovirus B19.

Raphael Wolfisberg, Nico Ruprecht, Christoph Kempf and Carlos Ros

Journal of Virological Methods 193 (2013) 215–225

Contents lists available at SciVerse ScienceDirect

Journal of Virological Methods

journal homepage: www.elsevier.com/locate/jviromet

Impaired genome encapsidation restricts the *in vitro* propagation of human parvovirus B19

Raphael Wolfisberg[a], Nico Ruprecht[a], Christoph Kempf[a,b], Carlos Ros[a,b,*]

[a] Department of Chemistry and Biochemistry, University of Bern, Freiestrasse 3, 3012 Bern, Switzerland
[b] CSL Behring AG, Wankdorfstrasse 10, 3000 Bern 22, Switzerland

Article history:
Received 7 March 2013
Received in revised form 24 May 2013
Accepted 3 June 2013
Available online 10 June 2013

Keywords:
Parvovirus B19
UT7/Epo cells
Erythroid progenitor cells
EPCs
VP1u
Hypoxia

A B S T R A C T

The lack of a permissive cell culture system hampers the study of human parvovirus B19 (B19V). UT7/Epo is one of the few established cell lines that can be infected with B19V but generates none or few infectious progeny. Recently, hypoxic conditions or the use of primary CD36+ erythroid progenitor cells (CD36+ EPCs) have been shown to improve the infection. These novel approaches were evaluated in infection and transfection experiments. Hypoxic conditions or the use of CD36+ EPCs resulted in a significant acceleration of the infection/transfection and a modest increase in the yield of capsid progeny. However, under all tested conditions, genome encapsidation was impaired seriously. Further analysis of the cell culture virus progeny revealed that differently to the wild-type virus, the VP1 unique region (VP1u) was exposed partially and was unable to become further externalized upon heat treatment. The fivefold axes pore, which is used for VP1u externalization and genome encapsidation, might be constricted by the atypical VP1u conformation explaining the packaging failure. Although CD36+ EPCs and hypoxia facilitate B19V infection, large quantities of infectious progeny cannot be generated due to a failure in genome encapsidation, which arises as a major limiting factor for the *in vitro* propagation of B19V.

1. Introduction

Human parvovirus B19 (B19V) is spread worldwide and typically causes a mild self-limiting infection in children known as *erythema infectiosum*. B19V has also been associated to myocarditis, acute and chronic arthropathies in adults, transient aplastic crisis and chronic anemia in individuals with altered immunologic or hematologic conditions, hydrops fetalis and intrauterine fetal death (Heegaard and Hornsleth, 1995; Heegaard and Brown, 2002; Servey et al., 2007).

Considering its worldwide distribution, prevalence and associated disorders, B19V is regarded as a prominent human pathogen and the only parvovirus undoubtedly linked to human disease. However, the experimental research with B19V is hampered seriously due to the lack of an appropriate and sufficiently permissive cell system to propagate the virus and study its biology. The reason for this is the rigorous replication requirements of the virus. B19V has an extraordinary tropism for erythroid progenitor cells in the bone marrow at a particular differentiation stage corresponding to BFU-E and CFU-E (Takahashi et al., 1990; Ozawa et al., 1986, 1987). The narrow tropism of B19V is mediated, at least in part, by its particular uptake mechanism. B19V utilizes globoside (Gb4Cer) as a primary attachment receptor, which is expressed in few cell types (Brown et al., 1993) and a co-receptor (Weigel-Kelley et al., 2003) to initiate the internalization process. However, cells expressing the required receptors and co-receptors are not always permissive, suggesting that the selective replication of B19V is determined by additional intracellular factors restricted to erythroid cells (Pallier et al., 1997; Brunstein et al., 2000; Gallinella et al., 2000; Guan et al., 2008; Chen et al., 2010; Luo et al., 2011). The high viremia that is typically associated to B19V acute infections, exceeding occasionally 10^{13} genome equivalents (geq) per ml of plasma (Kooistra et al., 2011), suggests that the virus can replicate efficiently in the target cells when all the required elements are present. However, despite continuous efforts, the specific cellular factors that control B19V infection in the natural target cells have not yet been reproduced adequately in an established cell line. Some erythropoietin-dependent leukemic cell lines, notably UT7/Epo (Shimomura et al., 1992) and KU812Ep6 (Miyagawa et al., 1999), have been shown to be semi-permissive to B19V infection, producing in general none or minor amounts of infectious progeny. The permissivity of non-erythroid cells, such as HepG2 cells has produced contradictory results (Caillet-Fauquet et al., 2004a; Bonvicini et al., 2008). Considering all these limitations, highly viremic donors without B19V neutralizing antibodies remain the only source of infectious B19V. Thus, the need to develop

* Corresponding author at: Department of Chemistry and Biochemistry, University of Bern, Freiestrasse 3, 3012 Bern, Switzerland. Tel.: +41 31 6314349; fax: +41 31 6314887.
E-mail address: carlos.ros@ibc.unibe.ch (C. Ros).

0166-0934/$ – see front matter © 2013 Elsevier B.V. All rights reserved.
http://dx.doi.org/10.1016/j.jviromet.2013.06.003

a cell culture method capable of producing large amounts of infectious B19V remains a major challenge.

Recently, the use of cells cultured under hypoxic conditions has been described as a promising method to produce high quantities of infectious particles (Caillet-Fauquet et al., 2004b; Pillet et al., 2004; Chen et al., 2011). Similarly, the use of *ex vivo* expanded CD36+ primary human erythroid progenitor cells (CD36+ EPCs), previous CD34+ *in vitro* preselection (Pillet et al., 2008; Wong et al., 2008), has also been described as a highly permissive system, based on the expression of B19V non-structural and capsid proteins. A simplified approach to generate CD36+ EPCs directly from ordinary blood samples, without *ex vivo* stem cell mobilization has been reported (Filippone et al., 2010). The combination of both approaches, primary CD36+ EPCs cultured under hypoxic conditions, has been shown to enhance remarkably B19V infection (Chen et al., 2011). Hypoxia, which mimics the oxygen microenvironment in the bone marrow, seems to promote B19V infection by the direct stimulating effect of HIF1α on the B19V p6 promoter (Pillet et al., 2004). However, an alternative HIF1α-independent mechanism based on STAT5A and MEK signaling has been proposed recently (Chen et al., 2011).

These novel approaches based on hypoxia and primary CD36+ EPCs have been compared systematically in infection and transfection experiments with the established erythroid cell line UT7/Epo. In all cases, a substantial amount of capsid progeny was obtained. The use of the novel approaches resulted in a significant acceleration of the infection and the augmentation in the number of infected cells resulting in a modest but noticeable increase in virus progeny production. However, in all tested cells and under all conditions genome encapsidation was impaired seriously generating an empty non-infectious virus progeny. Differently to the wild-type virus, the VP1 unique region (VP1u) of the virus progeny was exposed partially and upon heat treatment did not undergo the expected conformational change that renders VP1u fully externalized. The abnormal configuration and rigidity of VP1u, which utilizes the genome encapsidation portal for its externalization, might constrict the fivefold axes channel impeding the translocation of the viral genome into the pre-assembled capsid.

2. Materials and methods

2.1. Cells and viruses

UT7/Epo cells were maintained in Eagle's minimum essential medium (MEM) supplemented with 5% heat-inactivated fetal calf serum (FCS) and 2 U/ml of recombinant human erythropoietin (Epo; Janssen-Cilag, Midrand, South Africa) at 37 °C with 5% CO_2. For hypoxic conditions the oxygen tension was lowered to 1%. Cells with adherent phenotype were selected by removing the non-adherent cells in every passage. CD36+ erythroid progenitor cells (CD36+ EPCs) were obtained from ordinary blood samples and cultured as described previously (Filippone et al., 2010). A B19V-infected plasma sample (Genotype 1; CSL Behring AG, Charlotte, NC), without detectable B19V-specific IgM or IgG antibodies, was used as a source of native infectious virus. The virus was pelleted by ultracentrifugation through 20% (w/v) sucrose and the concentration of virions was determined by quantitative PCR (qPCR).

2.2. Antibodies and chemicals

Two human monoclonal antibodies (mAb), one directed to a conformational epitope in the major capsid protein VP2 (mAb 860-55D), which detects exclusively intact capsids, and the other against the N-terminal region of VP1, also known as VP1 unique region (VP1u) (mAb 1418), were provided by S. Modrow (Regensburg, Germany). These antibodies were produced from peripheral blood mononuclear cells of normal, healthy individuals with high titers of serum antibodies against B19 virus proteins (Gigler et al., 1999). A rabbit antibody against the C-terminal region of VP1u was described earlier (Bönsch et al., 2008). A mouse mAb against B19V capsids (mAb 521-5D) was purchased from Millipore (Billerica, MA). A globoside-specific mouse IgM mAb (AME-2) was provided by J. de Jong (The Netherlands Red Cross, Amsterdam, Netherlands). Mouse IgG mAb against Ku80 and CD49e were purchased from BD Biosciences (San Jose, CA). A mouse antibody against B19V proteins was obtained from US biologicals (Swampscott, MA). Chloroquine diphosphate (CQ) was purchased from Sigma (St. Louis, MO) and dissolved in water.

2.3. Flow cytometry

The presence of B19V receptors and co-receptors on the cell surface of UT7/Epo cells was analyzed quantitatively by flow cytometry. UT7/Epo cells were incubated with either an anti-Ku80 or an anti-Gb4Cer antibody at 4 °C for 1 h in PBS containing 2% fetal calf serum, followed by incubation with fluorescein isothiocyanate (FITC)-conjugated rat anti-mouse IgG or IgM, respectively (BD Biosciences). Additionally, UT7/Epo cells were stained with R-phycoerythrin conjugated anti-human CD49e (BD Biosciences). The cells were analyzed on a BD FacsCanto II (Becton Dickinson, San Jose, CA). Data acquisition and analysis were conducted with a software (BD FacsDiva, BD Biosciences).

2.4. Infection

UT7/Epo and primary CD36+ EPCs (3×10^5) cultured under normoxia or hypoxia (1% O_2) during 2 days, were infected with B19V at 10^4 geq per cell for 1 h at 4 °C. The cells were washed to remove unbound viruses and further incubated at 37 °C. At different post-infection (p.i.) times, cells and supernatants were collected. The cells were washed and processed for immunofluorescence (IF), immunoprecipitation (IP), as well as DNA and RNA extraction. The supernatant was used for IP and DNA extraction.

2.5. Transfection

A total of 5×10^6 UT7/Epo cells, cultured under normoxia or hypoxia (1% O_2) during 2 days, were transfected using the AMAXA nucleofector™ II device (Lonza, Cologne, Germany) following the manufacturer's instructions. Transfection was carried out with 5 μg of the B19V genome excised from a B19V infectious clone (pB19-M20) (Zhi et al., 2004) or with 2 μg of a GFP-control plasmid, using the T-20 program. As a transfection reagent, AMAXA™ Cell Line Nucleofector™ Kit R (Lonza) was used. After transfection, the cells were maintained in 20 ml of pre-warmed culture medium. A volume of 5 ml of fresh MEM culture medium supplemented with 5% FCS and Epo (2 U/ml) was added to the cells 24 h post-transfection (p.t.). At increasing times p.t., the cells and supernatant were collected for further analysis.

2.6. Quantitation of B19V DNA and NS1 mRNA

Total DNA was extracted from cells or from the supernatant by using the DNeasy blood and tissue kit (Qiagen, Valencia, CA). For the isolation of total mRNA, cells were transferred to RNase-free tubes (Safe-Lock Tubes 1.5 ml, Eppendorf Biopur) and washed twice with PBS. Total poly-A-mRNA was isolated with the Dynabeads mRNA direct kit (Roche Diagnostics, Mannheim, Germany). The RNA preparations were used for reverse transcription as described previously (Bönsch et al., 2010a). Amplification of DNA or cDNA and real-time detection of PCR products were performed by qPCR

with the iQ SYBR Green Supermix and the CFX96 device (Bio-Rad, Cressier, Switzerland). Primers used for amplification were described elsewhere (Bönsch et al., 2010a).

2.7. Immunoprecipitation of B19V particles and quantitation of virions

Viral particles were immunoprecipitated from cell extracts or from the supernatant of infected cells with a human mAb against intact capsids (860-55D) (Gigler et al., 1999). As reference control, a known amount of virions was added to the uninfected cell extracts or to the supernatant. After overnight incubation at 4 °C in the presence of 20 μl of protein G agarose beads (Santa Cruz Biotechnology, Heidelberg, Germany) the supernatant was discarded and the beads were washed four times with PBSA. Immunoprecipitated viral capsids were detected by SDS-PAGE. To verify the presence of the viral genome, DNA was extracted from the immunoprecipitated virions by using the DNeasy blood and tissue kit (Qiagen) and quantified as specified above.

2.8. Immunofluorescence

Cells or purified viruses were fixed on coverslips by using acetone/methanol (1:1 [v/v]) solution at −20 °C for 4 min. Following blocking with goat serum diluted in PBS (20% [v/v]), the samples were incubated with the primary antibodies in PBS containing 2% goat serum for 1 h at room temperature (RT). The samples were washed and the appropriate fluorescently labeled secondary antibody in 2% goat serum was added for 1 h at RT. Nuclei was stained with 4′,6-diamidino-2-phenylindole (DAPI). Mowiol supplemented with 2.5% 1,4-Diazabicyclo[2.2.2]octan (DABCO) was used to maintain the fluorescent signal. Samples were examined by confocal laser scanning microscopy (Axiovert 200M, Carl Zeiss A.G., Feldbach, Switzerland).

2.9. Fluorescence in situ DNA hybridization

The presence of newly replicated viral genomes in the infected cells was examined by fluorescence *in situ* DNA hybridization (FISH). Biotinylated probes specific for B19V DNA were generated from PCR products by nick translation (Roche), according to the manufacturer's instructions. The size of the hybridization probes was 200–500 nucleotides in length, as confirmed by agarose gel electrophoresis. Cells were fixed and immunostained with mAb 860-55D against capsids and incubated in a humid chamber at 37 °C for 18 h with a volume of 20 μl hybridization mix (5 ng/μl biotinylated probe in 60% deionised formamide, 300 mM NaCl, 20 mM sodium citrate, 10 mM EDTA, 25 mM NaH_2PO_4 pH 7.4, 5% dextran sulfate and 250 ng/μl sheared salmon sperm DNA). Subsequently, the cells were washed (50% deionized formamide, 25 mM NaCl and 2.5 mM sodium citrate pH 7.4) three times for 5 min at RT and once at 37 °C. The samples were blocked for 30 min with 1% blocking solution (Roche) in 150 mM NaCl, 100 mM Tris–HCl pH 7.4. Biotin was detected with avidin-rhodamine (Roche) 1:500 in blocking solution for 45 min. Finally, the cells were washed three times 10 min (200 mM Tris–HCl pH 7.4, 1.5 M NaCl and 0.05% Tween-20), mounted with mowiol supplemented with DABCO and examined by confocal laser scanning microscopy.

3. Results

3.1. General profile of B19V infection in UT7/Epo cells

UT7/Epo cells have been used extensively to study B19V infection. However, intracellular factors restrict severely the infection of B19V in these and other cells, resulting in the production of none or few infectious progeny (Pallier et al., 1997; Brunstein et al., 2000; Gallinella et al., 2000; Guan et al., 2008). In order to better identify which steps of the infection are deficient, different parameters of B19V infection in UT7/Epo cells have been analyzed. Analysis of the expression profile of B19V receptor and co-receptors over a period of six weeks showed a high and stable expression of Gb4Cer and CD49e along the specified period. In contrast, expression of Ku80, which may have a similar role to Gb4Cer in certain cells (Munakata et al., 2005), was not significant (Fig. 1A). IF microscopy examination of infected cells confirmed that B19V can attach and internalize cells, adopting the typical intracellular distribution around the microtubule organizing center (MTOC) observed in other parvovirus infections (Fig. 1B). The kinetics of viral transcription and replication were analyzed quantitatively. The synthesis of viral RNA (NS1 mRNA) was already detectable by 3 h p.i. and reached a plateau by 24 h p.i. (Fig. 1C). Viral replication started later and reached a plateau by the third day p.i. (Fig. 1D). Expression of viral proteins became detectable after 24 h and reached a plateau after 2 days (Fig. 1E). Immunoprecipitation at 3 days p.i. with an antibody against intact viral particles (mAb 860-55D) (Gigler et al., 1999) demonstrated that virus assembly occurred and that a significant amount of capsid progeny was produced (Fig. 1F). Quantitative determination of the viral DNA from the immunoprecipitated capsids revealed that the virus progeny was essentially empty (Fig. 1G). Mature virion progeny was not either detected in the supernatant of the infected cells (Fig. 1H). These results together indicate that despite the substantial amount of capsid progeny produced, deficiencies in genome packaging and capsid egress limit the progression of B19V infection in UT7/Epo cells.

3.2. B19V infection of UT7/Epo cells, under normoxia or hypoxia, generates mostly empty capsids

Infected cells were collected at progressive days, washed and lysed. Viral particles were immunoprecipitated from the cell lysate with the antibody 860-55D, against assembled capsids. The results confirmed that under hypoxic conditions, the capsid progeny was more abundant but also appeared earlier (after 48 h p.i. under normoxia and after 24 h p.i. under hypoxia) (Fig. 2A and B). These results confirmed previous observations indicating that hypoxia enhances B19V infection (Caillet-Fauquet et al., 2004b; Pillet et al., 2004; Chen et al., 2011). The virus progeny generated under hypoxic or normoxic conditions was further characterized. The amount of viral genomes in the immunoprecipitated viral particles from the experiment shown in Fig. 2A and B was analyzed quantitatively. The results revealed that independently of the oxygen environment, a limited number of progeny capsids (<1% of the reference control) contained the viral DNA (Fig. 2C and D). Quantitation of the viral DNA in the supernatant of the infected cells showed no increase over the background signal (day 0 p.i.) under normoxia and modestly under hypoxic conditions (Fig. 2E and F). Capsid proteins in the supernatant were undetectable by IP and Western blot (data not shown). These results indicate that although hypoxic conditions result in the acceleration of the infection and an augmented capsid production, the improvement of the genome encapsidation step was not significant.

3.3. Hypoxia enhances significantly the transfection efficiency, however genome packaging and egress remained restricted

In a control transfection experiment in UT7/Epo cells, the oxygen level did not influence the transfection efficiency with a control plasmid expressing green fluorescent protein (GFP) (Fig. 3A). However, the transfection efficiency increased drastically under hypoxic conditions with an infectious clone of B19V (pB19-M20)

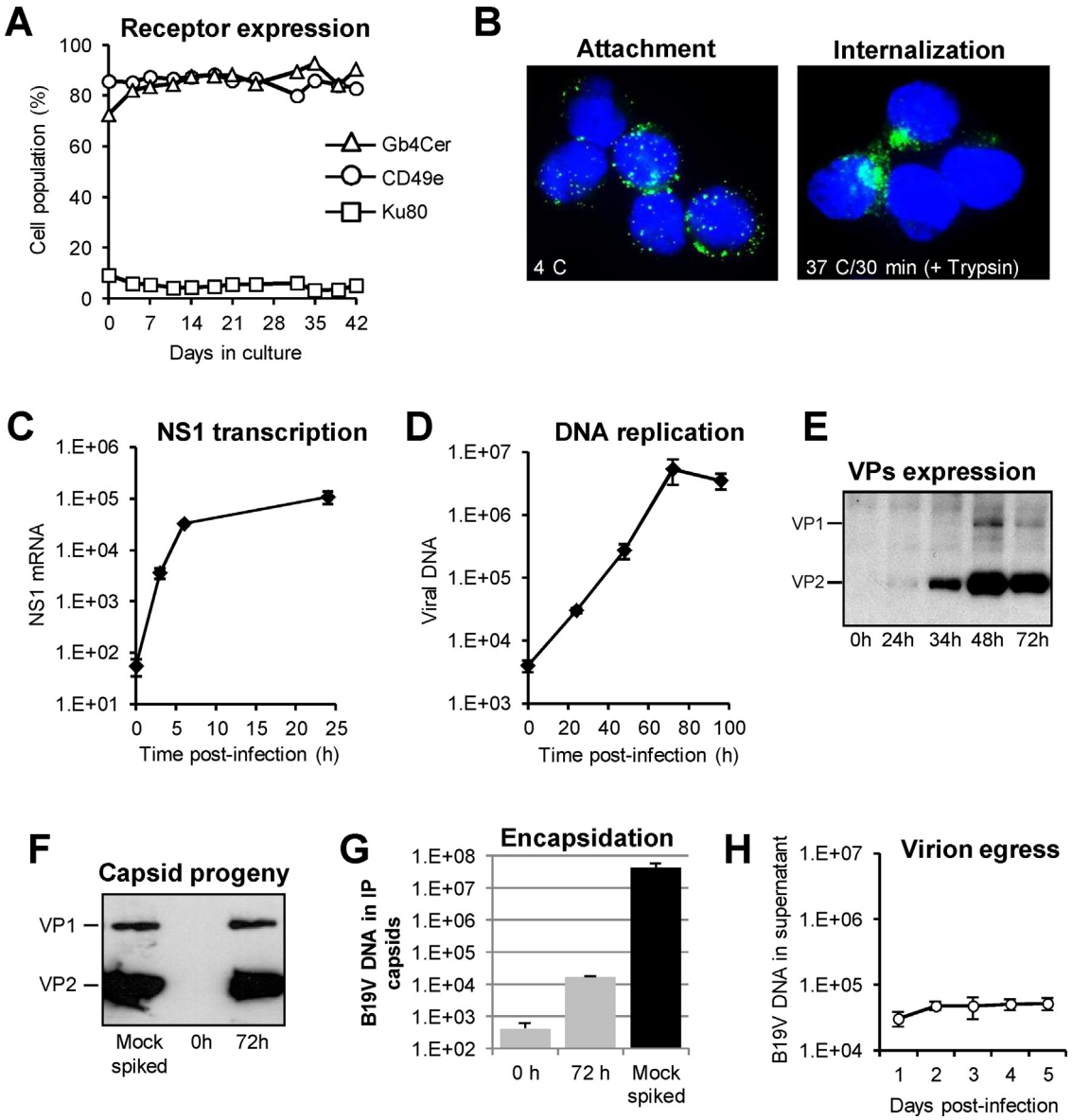

Fig. 1. Characterization of B19V infection in UT7/Epo cells. (A) Expression of B19V-related receptors in UT7/Epo cells. The presence of B19V receptors and co-receptors on the cell surface of UT7/Epo cells was quantitatively analyzed by flow cytometry during a period of 6 weeks. (B) Binding and internalization of B19V in UT7/Epo cells. B19V was added to the cells at 4 °C for 2 h, washed, fixed and stained with an antibody against intact capsids. For internalization, the cells were further incubated for 30 min at 37 °C, washed and trypsinized to remove uninternalized particles. (C) Kinetics of NS1 mRNA synthesis in infected cells. At increasing times p.i., total mRNA was isolated and NS1 mRNA quantified. Samples taken 10 min p.i. served as background controls. (D) Kinetics of viral DNA replication. At increasing times p.i., total DNA was isolated and viral DNA quantified. Samples taken prior to virus internalization served as background controls. (E) Kinetics of B19V capsid proteins expression. (F) Production of assembled capsid progeny in UT7/Epo cells. B19V capsids were immunoprecipitated from cell extracts with mAb 860-55D against intact capsids. As a reference control, B19V (4×10^{10}) was added to mock-infected cell extracts. (G) B19V capsids were immunoprecipitated and B19V DNA was quantified. As a reference control, B19V (4×10^{10} virions) was added to mock-infected cell extracts. (H) Quantitation of virus egress. B19V DNA was quantified from the supernatant of the infected cells.

(Fig. 3B). Immunoprecipitation experiments confirmed that assembled capsids were generated (Fig. 3C) and similarly to the infection experiments, progeny capsids were slightly more abundant and appeared earlier under hypoxic conditions.

As shown in Fig. 3D, at progressive times p.t. no viral DNA above the input signal was detected in the immunoprecipitated capsids. Additionally, virions were not detectable in the supernatant of the transfected cells (Fig. 3E).

3.4. Chloroquine enhances B19V infection in UT7/Epo cells but has no influence in genome encapsidation and egress

It has been shown previously that chloroquine (CQ) enhances B19V infection. In the presence of CQ, an increased production of viral DNA, RNA and proteins was observed and the infection was accelerated (Bönsch et al., 2010b). The production of mature virions in CQ-treated UT7/Epo cells was examined. The results confirmed, that in the presence of CQ, an increased amount of assembled capsids was produced (Fig. 4A). However, similar to untreated cells, most of the progeny capsids remained empty (Fig. 4B). Viral DNA or capsid proteins were not detected in the supernatant of infected cells (data not shown).

3.5. B19V infection is enhanced in CD36+ EPCs, in particular under hypoxia, but genome encapsidation remains restricted

Immunofluorescence microscopy examination of infected primary CD36+ EPCs confirmed that B19V can attach and internalize

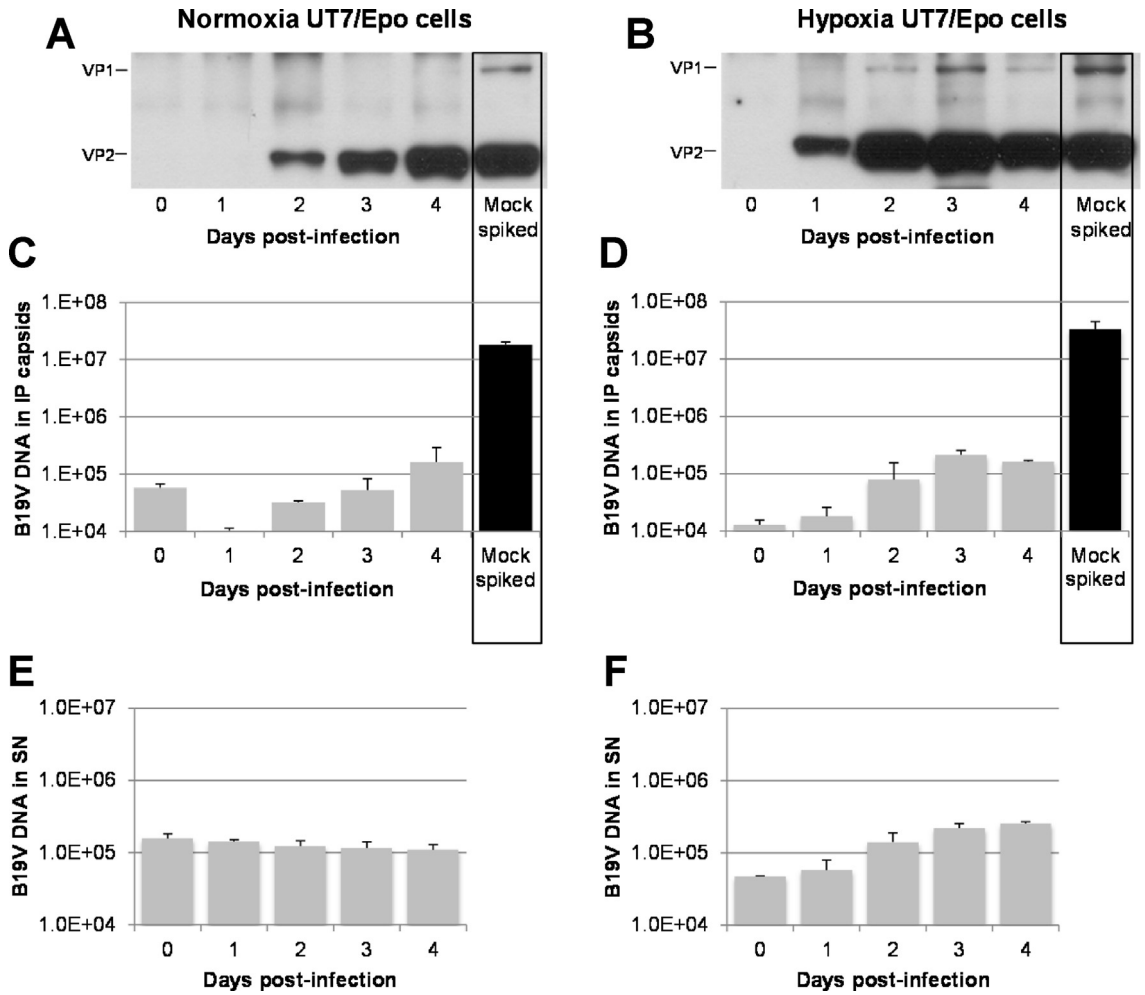

Fig. 2. Capsid progeny and quantitation of virions in UT7/Epo cells. Cells (3×10^5) were infected with B19V under normoxia or hypoxia. At progressive times p.i., the supernatant was collected and the cells were lysed. (A and B) B19V capsids were immunoprecipitated from the cell extracts with mAb 860-55D. As a reference control, B19V (4×10^{10}) was added to mock-infected cell extracts. (C and D) B19V DNA was quantified from the immunoprecipitated capsids. As a reference control, B19V (4×10^{10} virions) was added to mock-infected cell extracts. (E and F) B19V DNA was quantified from the supernatant of the infected cells. Data are the mean ± SD of two independent experiments.

EPCs without noticeable differences to UT7/Epo cells or between normoxic and hypoxic conditions (Fig. 5A). However, the oxygen environment had an important influence in the number of cells infected by B19V. By 2 days p.i., the number of UT7/Epo cells with detectable capsid progeny was 1–5% and 15–20% under normoxia and hypoxia, respectively. In CD36+ EPCs, the number of infected cells increased to approximately 25% under normoxia and above 70% under hypoxic conditions (Fig. 5B).

Immunoprecipitation experiments with the antibody 860-55D (against intact capsids) at progressive days p.i. showed, that regardless the oxygen conditions, progeny capsids appeared earlier in CD36+ EPCs than in UT7/Epo cells. While in UT7/Epo cells, capsid progeny production reached a plateau on day 4 under normoxia and on day 2–3 under hypoxia, in CD36+ EPCs, maximal capsid progeny was observed already after 24 h p.i. (compare Fig. 6A and B and Fig. 2A and B). The amount of viral DNA in the immunoprecipitated samples from the experiment shown in Fig. 6A and B was analyzed quantitatively. The results revealed that a limited number of capsids containing the viral DNA were produced after 24 h p.i. and did not increase subsequently (Fig. 6C and D). The presence of viral DNA in the supernatant increased and reached similarly a plateau already after 24 h p.i. (Fig. 6E and F).

Capsid progeny was detectable in the supernatant of infected EPCs, in particular under hypoxic conditions (Fig. 7A and B). However, quantitation of their DNA content and comparison with the reference control revealed that only a modest proportion of the particles represented mature infectious virions (Fig. 7C and D). The IP of capsid-associated DNA increased and reached a plateau by 24 h p.i. At this time, the capsid progeny was undetectable under normoxia and hardly detectable under hypoxia (Fig. 7A and B). Therefore, the increase of capsid progeny observed in the following days represented essentially empty particles. These results indicate that despite the augmented and earlier production of virus progeny, the deficient packaging step remains the limiting factor for the propagation of B19V in CD36+ EPCs.

3.6. Intracellular distribution of viral genomes and capsids

The presence and distribution of the viral genomes and capsids in the infected UT7/Epo cells was examined by FISH. In some cells, assembled capsids and viral genomes colocalized within large intranuclear clusters (Fig. 8A, panel i) resembling the nuclear compartments described earlier in AAV, containing non-structural proteins, capsids, and viral genomes and where presumably encapsidation takes place (Hunter and Samulski, 1992; Wistuba et al., 1997). However, in a larger proportion of cells the viral genomes appeared isolated in the nucleus, while the assembled capsids were detected in the cytoplasm (Fig. 8A, panel ii).

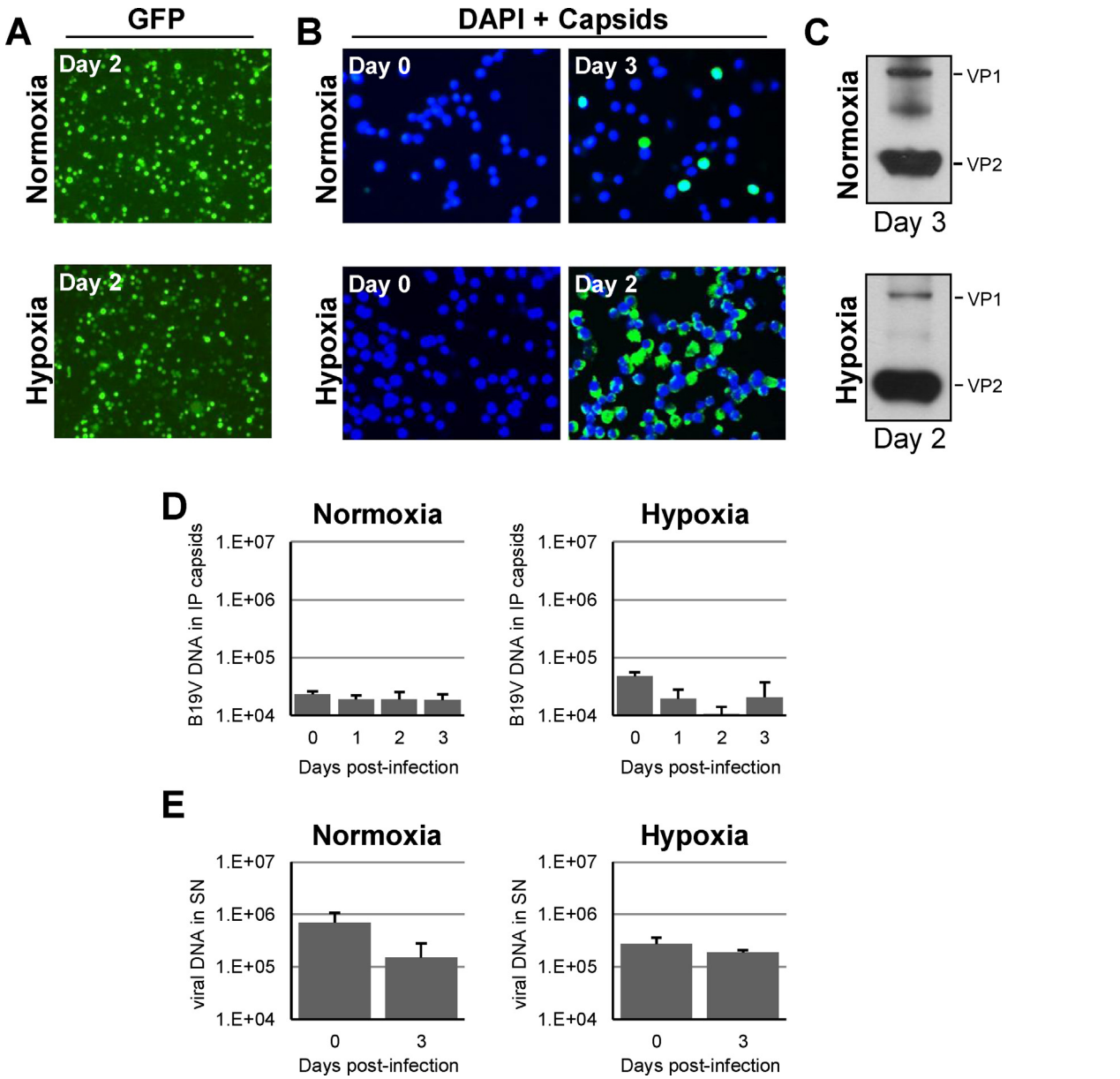

Fig. 3. Transfection of UT7/Epo cells with a B19V infectious clone under normoxia and hypoxia. (A) Transfection of UT7/Epo cells with a control plasmid expressing GFP is not influenced by normoxia or hypoxia. (B) Detection of B19V capsids by IF following transfection with a B19V infectious clone (pB19-M20). (C) Detection of B19V capsids by IP with mAb 860-55D from pB19-M20 transfected cells. (D) At progressive days p.i. B19V capsids were immunoprecipitated from cell lysates and B19V DNA was quantified. (E) B19V DNA was quantified from the supernatant of the infected cells. Data are the mean ± SD for two independent experiments.

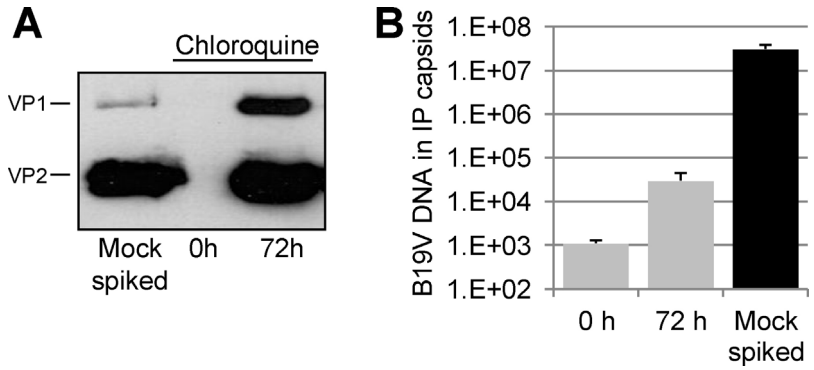

Fig. 4. Effect of chloroquine (CQ) in B19V infection in UT7/Epo cells. (A) Production of capsid progeny in UT7/Epo cells treated with CQ (25 μM). B19V capsids were immunoprecipitated from the cell extracts with mAb 860-55D. As a reference control, B19V (4×10^{10}) was added to mock-infected cell extracts. The production of capsid progeny in untreated UT7/Epo cells is shown in Fig. 1F. (B) B19V DNA was quantified from the immunoprecipitated capsids. As a reference control, B19V (4×10^{10} virions) was added to mock-infected cell extracts. Data are the mean ± SD for two independent experiments.

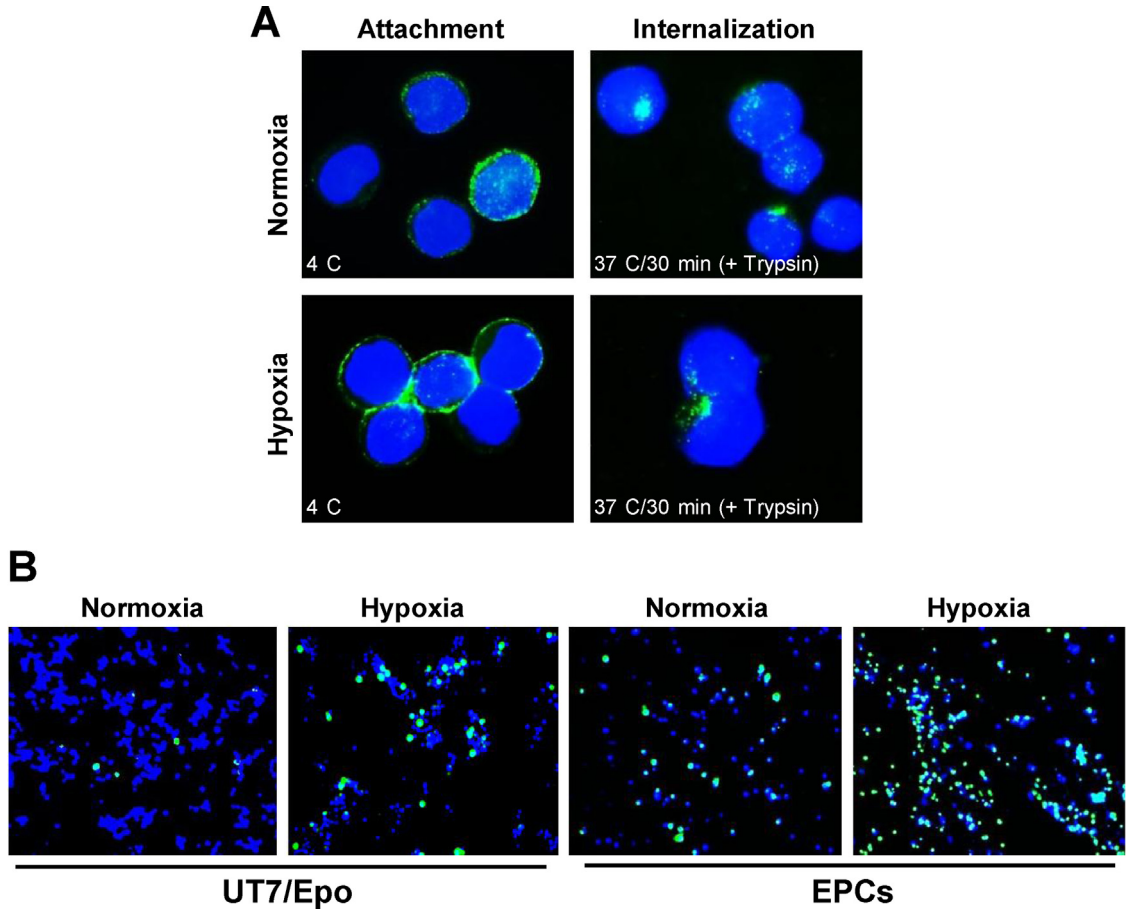

Fig. 5. Attachment, internalization and infection of B19V in EPCs under normoxia and hypoxia. Cells (3×10^5) were infected with B19V under normoxia or hypoxia. (A) Binding and internalization of B19V in EPCs. B19V was added to the cells at 4 °C for 1 h, washed, fixed and stained with an antibody against intact capsids. For internalization, the cells were further incubated for 30 min at 37 °C, washed and trypsinized to remove uninternalized particles. (B) Detection of virus progeny by IF 2 days p.i. in UT7/Epo cells and EPCs cultured under normoxic and hypoxic conditions.

3.7. VP1u conformation in the virus progeny differs from that of wild-type virus

The pores at the fivefold symmetry axis are the portals for the encapsidation of the viral genome but also for the externalization of VP1u. The fivefold cylinder is narrow and constrictions of the channel impair the encapsidation of the viral genome and the externalization of VP1u (Farr and Tattersall, 2004; Bleker et al., 2005, 2006; Plevka et al., 2011). Examination of the VP1u conformation in the mostly empty virus progeny revealed, that differently to the wild-type virus, VP1u was partially exposed. The most N-terminal part was accessible to antibodies, while the C-terminal region remained internal and inaccessible (Fig. 8B and C). Similar to other parvoviruses (Cotmore et al., 1999; Vihinen-Ranta et al., 2002), exposure to mild temperature triggers the externalization of the N-terminal and C-terminal regions of VP1u from B19V without capsid disassembly (Ros et al., 2006). In clear contrast to the wild-type virus, heat treatment did not trigger the externalization of the C-terminal region of VP1u from the capsid progeny generated under normoxia and only discretely from capsids generated under hypoxia (Fig. 8D). Therefore, the failure to encapsidate the viral genome is possibly due to the constriction of the fivefold axis channel by a partially exposed and inflexible VP1u.

4. Discussion

Discovered in 1975 (Cossart et al., 1975), today B19V is recognized as a major human pathogen involved in multiple syndromes. However, the lack of a suitable cell culture system or an animal model restricts the availability of infectious virus and hampers seriously the studies with B19V. The virus has an extraordinary tropism for human erythroid progenitor cells (EPCs) in the bone marrow (Mortimer et al., 1983) where it can infect cells at the BFU-E and CFU-E stages of differentiation (Takahashi et al., 1990). During a natural infection B19V is able to replicate efficiently in the target cells, as judged by the typical high viremia observed in the infected individuals. However, the efficient B19V replication *in vivo* has not yet been mimicked *in vitro* with an established cell line, indicating the existence of highly restricted and still poorly understood cellular factors required for B19V replication. Some erythroleukemia cell lines, such as UT7/Epo (Shimomura et al., 1992) and KU812Ep6 (Miyagawa et al., 1999), have been shown to support B19V replication to a certain level, but none of them can produce significant quantities of infectious progeny. The human megakaryoblastic cell line UT7/Epo, has been shown to be the most permissive system for the *in vitro* replication of B19V (Wong and Brown, 2006) and it is used widely to study B19V infection.

The reason for the defective replication of B19V in these cells has been shown to be multifactorial. Restrictions occur already at the cell surface, by the variable and limited expression of receptors and co-receptors required for binding and internalization of B19V (Brown et al., 1993; Munakata et al., 2005; Weigel-Kelley et al., 2003), but also by required intracellular factors restricted mainly to the erythroid lineage. Those intracellular factors can operate at the level of transcription, controlling the generation of sufficient full-length capsid-encoding transcripts (Guan et al., 2008; Liu et al.,

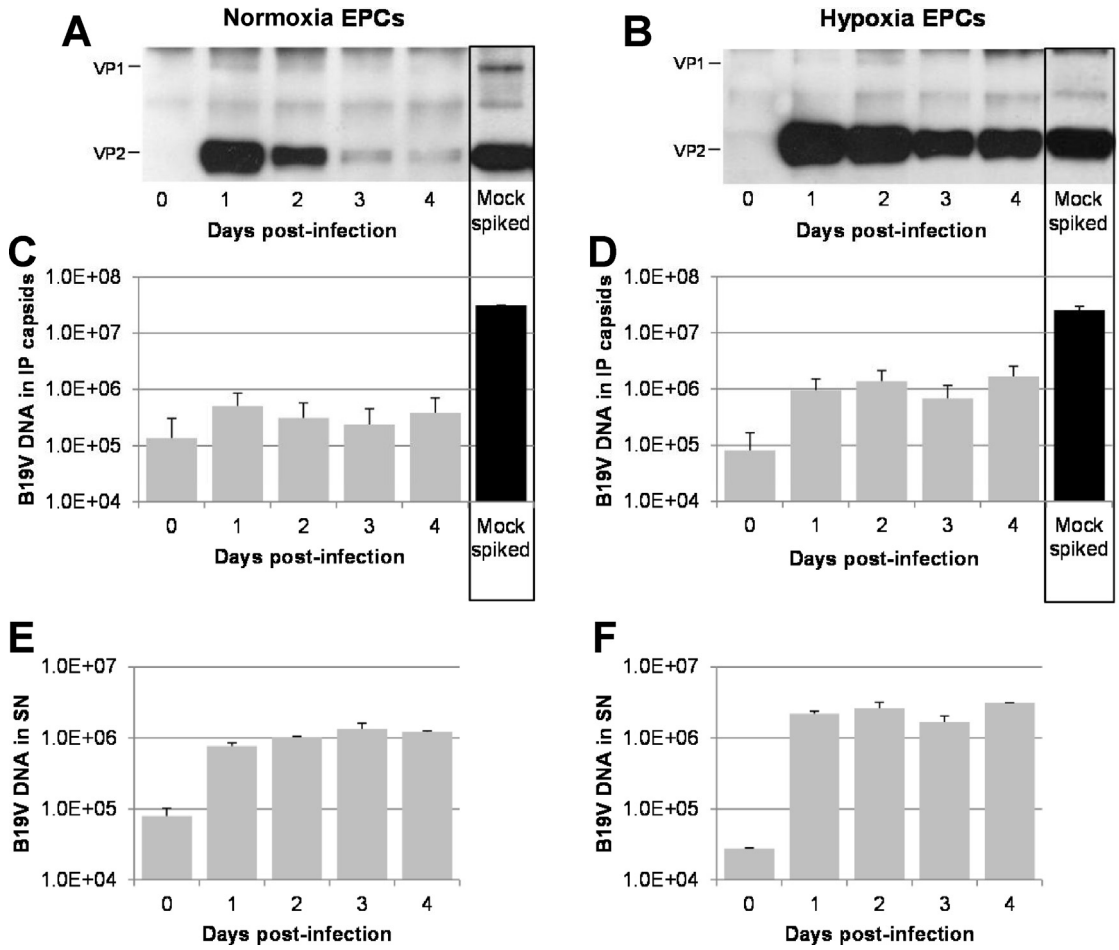

Fig. 6. Capsid progeny and quantitation of virions in EPCs. Cells (3×10^5) were infected with B19V under normoxia or hypoxia. At progressive times p.i., the supernatant was collected and the cells were lysed. (A and B) B19V capsids were immunoprecipitated from the cell extracts with mAb 860-55D, against intact capsids. As a reference control, B19V (4×10^{10}) was added to mock-infected cell extracts. (C and D) B19V DNA was quantified from the immunoprecipitated capsids. As a reference control, B19V (4×10^{10} virions) was added to mock-infected cell extracts. (E and F) B19V DNA was quantified from the supernatant of the infected cells. Data are the mean ± SD of two independent experiments.

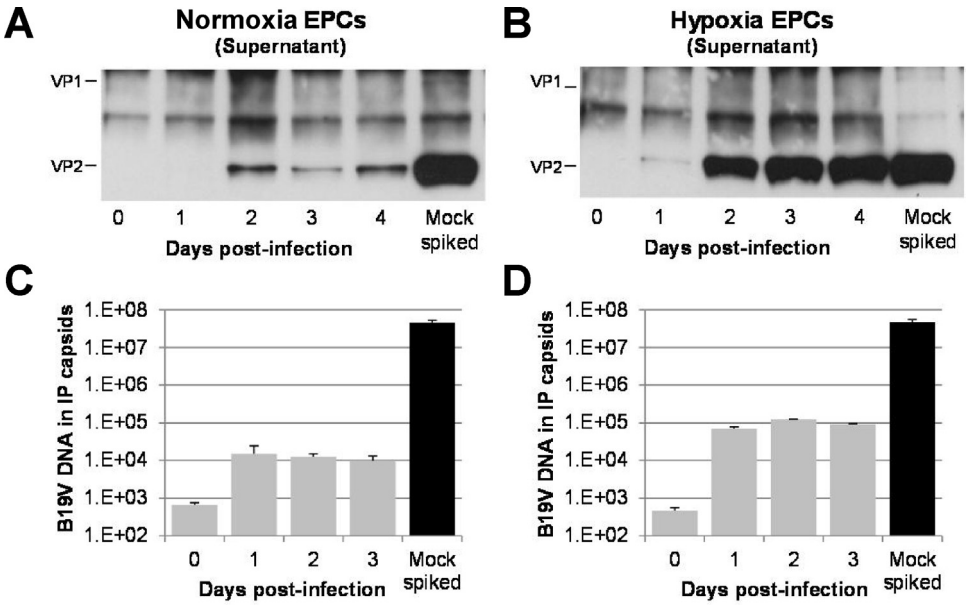

Fig. 7. Virus egress in EPCs. Cells (3×10^5) were infected with B19V under normoxia or hypoxia. (A and B) At progressive times p.i., B19V capsids were immunoprecipitated from the cell supernatant with mAb 860-55D. As a reference control, B19V (4×10^{10}) was added to mock-infected cell supernatant. (C and D) B19V capsids were immunoprecipitated and B19V DNA was quantified. As a reference control, B19V (4×10^{10} virions) was added to mock-infected cell supernatant. Data are the mean ± SD of two independent experiments.

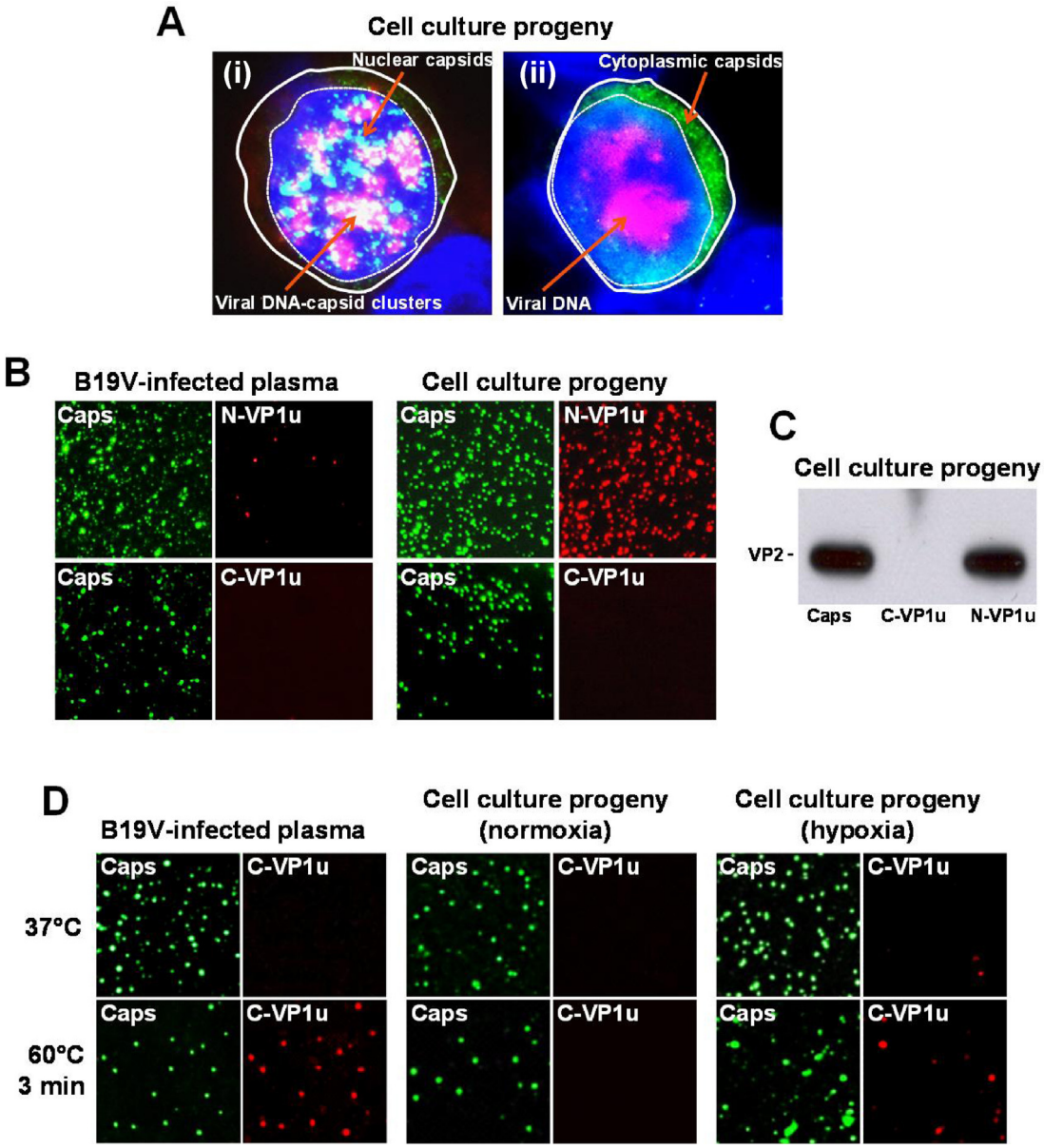

Fig. 8. Intracellular distribution of capsids and viral genomes and VP1u conformation in the capsid progeny. (A) Simultaneous detection of viral genomes and capsids in infected UT7Epo cells by FISH. Two representative cells are shown. (i) In some cells, B19V genomes and capsids were detectable in large clusters in the nucleus. (ii) In a larger proportion of cells, viral genomes were detected isolated in the nucleus while capsids were detected in the cytoplasm. (B) VP1u conformation in the plasma-derived virus differs from that of the cell culture progeny (UT7/Epo cells). Plasma-derived virus and cell culture progeny were concentrated by sucrose cushion centrifugation, spotted onto coverslips, fixed and detected by IF with mAb 860-55D or mAb 521-5D (Caps) and antibodies against the N-terminal and C-terminal regions of VP1u. (C) Immunoprecipitation of the cell culture progeny (UT7/Epo cells, 3 days p.i.) with mAb 860-55D (Capsids) and antibodies against the N-terminus and C-terminus of VP1u. (D) Flexibility of VP1u in the plasma-derived virus and cell culture progeny obtained under normoxia or hypoxia. Viruses were untreated (37 °C) or heat-treated (60 °C for 3 min) to trigger the exposure of VP1u and detected by IF with the indicated antibodies.

1992). In non-permissive cells the majority of viral mRNAs encode for NS1, with only limited production of the capsid-encoding transcripts. NS1 causes cell death by its cytotoxic or apoptotic characteristics (Moffatt et al., 1998). In contrast, more B19V RNAs are read through the multiple polyadenylation sites in permissive cells, which results in sufficient full-length capsid-encoding mRNAs (Liu et al., 1992). Studies have also shown that B19V replication and transcription were restricted to a small subset of cells but without production of capsid proteins, while in other cells, the single-stranded viral DNA was not converted to the double-stranded form (Gallinella et al., 2000). All the described restrictions at early (receptor/co-receptor) and late (replication/transcription) stages of the infection result in none or limited production of virus progeny.

Recently, two novel approaches based on hypoxic conditions (Caillet-Fauquet et al., 2004b; Pillet et al., 2004) and the use of *ex vivo* expanded CD36+ primary human erythroid progenitor cells (CD36+ EPCs), previous CD34+ *in vitro* preselection (Pillet et al., 2008; Wong et al., 2008), or directly from unselected peripheral blood mononuclear cells (Filippone et al., 2010), have been shown to improve B19V infection. The obtained results are in agreement with previous observations, which showed that B19V replicates better in CD36+ EPCs, in particular under hypoxia (Chen et al., 2011). However, despite these improvements, the final genome encapsidation step was still insufficient, producing abundant but mostly non-infectious empty capsids. In the study by Chen et al. (2011), the use of EPCs under hypoxia was shown to improve B19V infection, however large quantities of infectious virus were not

recovered from the supernatant of the infected cells, as it should be expected for a lytic virus. Therefore, CD36+ EPCs cannot yet be considered as a highly permissive cell culture system to propagate B19V and a robust source of infectious virus. Moreover, compared to UT7/Epo cells, the generation of primary CD36+ EPCs remains time-consuming, requires large quantities of expensive growth factors and the permissivity to B19V is limited within a narrow and variable time-frame when B19V receptor and co-receptors are expressed in concert with a favorable intracellular microenvironment (Wong et al., 2008).

Parvoviruses pack their single-stranded, linear DNA genome into the pre-assembled capsids in the nucleus (Cotmore and Tattersall, 2005; King et al., 2001; Timpe et al., 2005). The helicase activity of the parvovirus nonstructural protein, which is present in the encapsidation complexes, functions as a molecular motor to translocate the viral genome into the empty capsid through the fivefold axes pore, a process that is also mediated by the terminal telomeric structures of the viral genome (Cotmore and Tattersall, 2005; King et al., 2001). Besides genome encapsidation, the channels at the fivefold symmetry axis are also used for the externalization of VP1u during the infection process (Bleker et al., 2005, 2006; Cotmore and Tattersall, 2012; Farr and Tattersall, 2004; Plevka et al., 2011). The channel is narrow and minor modifications of its diameter result in defective genome encapsidation and VP1u externalization (Bleker et al., 2005; Cotmore and Tattersall, 2012). Therefore, specific capsid and genome conformations play a critical role in the packaging step. VP1u from parvoviruses is not accessible, but can become exposed *in vitro* by mild heat or low pH treatments and *in vivo* during the intracellular trafficking of the virus (Cotmore et al., 1999; Kronenberg et al., 2005; Mani et al., 2006; Ros et al., 2006; Vihinen-Ranta et al., 2002) or upon receptor binding in the case of B19V (Bönsch et al., 2010a). In clear contrast to natural plasma-derived virus, VP1u was exposed partially in the capsid progeny. While the most N-terminal region was externalized and accessible to antibodies, the C-terminal region remained internal (Fig. 8). This particular conformation was irreversible and did not change upon heat treatment. The aberrant conformation and rigidity of VP1u might explain the encapsidation failure in semi-permissive cell systems. Further studies will elucidate whether the VP1u conformation in the virus progeny is due to an aberrant assembly or the lack of a final maturation step.

5. Conclusions

When compared to UT7/Epo cells and normoxia, hypoxic conditions or the use of CD36+ EPCs resulted in a significant acceleration of the infection/transfection, an increase in the number of infected cells and a modest increase in the yield of capsid progeny. However, despite these improvements, genome encapsidation was impaired seriously under all tested conditions and cells. The fivefold axes channel might be constricted in the virus progeny by the atypical partial exposure of VP1u hindering the packaging step, which arises as a major limiting factor for the *in vitro* propagation of B19V.

Acknowledgments

We are grateful to M. Bärtschi for performing the flow cytometry assay and S. Bieli for the technical assistance in the fluorescence *in situ* DNA hybridization experiments.

References

Bleker, S., Pawlita, M., Kleinschmidt, J.A., 2006. Impact of capsid conformation and Rep-capsid interactions on adeno-associated virus type 2 genome packaging. J. Virol. 80, 810–820.
Bleker, S., Sonntag, F., Kleinschmidt, J.A., 2005. Mutational analysis of narrow pores at the fivefold symmetry axes of adeno-associated virus type 2 capsids reveals a dual role in genome packaging and activation of phospholipase A2 activity. J. Virol. 79, 2528–2540.
Bönsch, C., Zuercher, C., Lieby, P., Kempf, C., Ros, C., 2010a. The globoside receptor triggers structural changes in the B19 virus capsid that facilitate virus internalization. J. Virol. 84, 11737–11746.
Bönsch, C., Kempf, C., Mueller, I., Manning, L., Laman, M., Davis, T.M., Ros, C., 2010b. Chloroquine and its derivatives exacerbate B19V-associated anemia by promoting viral replication. PLoS Negl. Trop. Dis. 4 (4), e669.
Bönsch, C., Kempf, C., Ros, C., 2008. Interaction of parvovirus B19 with human erythrocytes alters virus structure and cell membrane integrity. J. Virol. 82, 11784–11791.
Bonvicini, F., Filippone, C., Manaresi, E., Zerbini, M., Musiani, M., Gallinella, G., 2008. HepG2 hepatocellular carcinoma cells are a non-permissive system for B19 virus infection. J. Gen. Virol. 89, 3034–3038.
Brown, K.E., Anderson, S.M., Young, N.S., 1993. Erythrocyte P antigen: cellular receptor for B19 parvovirus. Science 262, 114–117.
Brunstein, J., Söderlund-Venermo, M., Hedman, K., 2000. Identification of a novel RNA splicing pattern as a basis of restricted cell tropism of erythrovirus B19. Virology 274, 284–291.
Caillet-Fauquet, P., Di Giambattista, M., Draps, M.L., Hougardy, V., de Launoit, Y., Laub, R., 2004a. An assay for parvovirus B19 neutralizing antibodies based on human hepatocarcinoma cell lines. Transfusion 44, 1340–1343.
Caillet-Fauquet, P., Draps, M.L., Di Giambattista, M., de Launoit, Y., Laub, R., 2004b. Hypoxia enables B19 erythrovirus to yield abundant infectious progeny in a pluripotent erythroid cell line. J. Virol. Methods 121, 145–153.
Chen, A.Y., Kleiboeker, S., Qiu, J., 2011. Productive parvovirus B19 infection of primary human erythroid progenitor cells at hypoxia is regulated by STAT5A and MEK signaling but not HIFα. PLoS Pathog. 7 (6), e1002088.
Chen, A.Y., Guan, W., Lou, S., Liu, Z., Kleiboeker, S., Qiu, J., 2010. Role of erythropoietin receptor signaling in parvovirus B19 replication in human erythroid progenitor cells. J. Virol. 84, 12385–12396.
Cossart, Y.E., Field, A.M., Cant, B., Widdows, D., 1975. Parvovirus-like particles in human sera. Lancet 1, 72–73.
Cotmore, S.F., Tattersall, P., 2012. Mutations at the base of the icosahedral five-fold cylinders of minute virus of mice induce 3′-to-5′ genome uncoating and critically impair entry functions. J. Virol. 86, 69–80.
Cotmore, S.F., Tattersall, P., 2005. Encapsidation of minute virus of mice DNA: aspects of the translocation mechanism revealed by the structure of partially packaged genomes. Virology 336, 100–112.
Cotmore, S.F., D'abramo Jr., A.M., Ticknor, C.M., Tattersall, P., 1999. Controlled conformational transitions in the MVM virion expose the VP1 N-terminus and viral genome without particle disassembly. Virology 254, 169–181.
Farr, G.A., Tattersall, P., 2004. A conserved leucine that constricts the pore through the capsid fivefold cylinder plays a central role in parvoviral infection. Virology 323, 243–256.
Filippone, C., Franssila, R., Kumar, A., Saikko, L., Kovanen, P.E., Söderlund-Venermo, M., Hedman, K., 2010. Erythroid progenitor cells expanded from peripheral blood without mobilization or preselection: molecular characteristics and functional competence. PLoS One 5 (3), e9496.
Gallinella, G., Manaresi, E., Zuffi, E., Venturoli, S., Bonsi, L., Bagnara, G.P., Musiani, M., Zerbini, M., 2000. Different patterns of restriction to B19 parvovirus replication in human blast cell lines. Virology 278, 361–367.
Gigler, A., Dorsch, S., Hemauer, A., Williams, C., Kim, S., Young, N.S., Zolla-Pazner, S., Wolf, H., Gorny, M.K., Modrow, S., 1999. Generation of neutralizing human monoclonal antibodies against parvovirus B19 proteins. J. Virol. 73, 1974–1979.
Guan, W., Cheng, F., Yoto, Y., Kleiboeker, S., Wong, S., Zhi, N., Pintel, D.J., Qiu, J., 2008. Block to the production of full-length B19 virus transcripts by internal polyadenylation is overcome by replication of the viral genome. J. Virol. 82, 9951–9963.
Heegaard, E.D., Brown, K.E., 2002. Human parvovirus B19. Clin. Microbiol. Rev. 15, 485–505.
Heegaard, E.D., Hornsleth, A., 1995. Parvovirus: the expanding spectrum of disease. Acta Paediatr. 84, 109–117.
Hunter, L.A., Samulski, R.J., 1992. Colocalization of adeno-associated virus Rep and capsid proteins in the nuclei of infected cells. J. Virol. 66, 317–324.
King, J.A., Dubielzig, R., Grimm, D., Kleinschmidt, J.A., 2001. DNA helicase-mediated packaging of adeno-associated virus type 2 genomes into preformed capsids. EMBO J. 20, 3282–3291.
Kooistra, K., Mesman, H.J., de Waal, M., Koppelman, M.H., Zaaijer, H.L., 2011. Epidemiology of high-level parvovirus B19 viraemia among Dutch blood donors, 2003–2009. Vox Sang. 100, 261–266.
Kronenberg, S., Bottcher, B., von der Lieth, C.W., Bleker, S., Kleinschmidt, J.A., 2005. A conformational change in the adeno-associated virus type 2 capsid leads to the exposure of hidden VP1N termini. J. Virol. 79, 5296–5303.
Liu, J.M., Green, S.W., Shimada, T., Young, N.S., 1992. A block in full-length transcript maturation in cells nonpermissive for B19 parvovirus. J. Virol. 66, 4686–4692.

Luo, Y., Lou, S., Deng, X., Liu, Z., Li, Y., Kleiboeker, S., Qiu, J., 2011. Parvovirus B19 infection of human primary erythroid progenitor cells triggers ATR-Chk1 signaling, which promotes B19 virus replication. J. Virol. 85, 8046–8055.
Mani, B., Baltzer, C., Valle, N., Almendral, J.M., Kempf, C., Ros, C., 2006. Low pH-dependent endosomal processing of the incoming parvovirus minute virus of mice virion leads to externalization of the VP1 N-terminal sequence (N-VP1), N-VP2 cleavage, and uncoating of the full-length genome. J. Virol. 80, 1015–1024.
Miyagawa, E., Yoshida, T., Takahashi, H., Yamaguchi, K., Nagano, T., Kiriyama, Y., Okochi, K., Sato, H., 1999. Infection of the erythroid cell line, KU812Ep6 with human parvovirus B19 and its application to titration of B19 infectivity. J. Virol. Methods 83, 45–54.
Moffatt, S., Yaegashi, N., Tada, K., Tanaka, N., Sugamura, K., 1998. Human parvovirus B19 nonstructural (NS1) protein induces apoptosis in erythroid lineage cells. J. Virol. 72, 3018–3028.
Mortimer, P.P., Humphries, R.K., Moore, J.G., Purcell, R.H., Young, N.S., 1983. A human parvovirus-like virus inhibits haematopoietic colony formation in vitro. Nature 302, 426–429.
Munakata, Y., Saito-Ito, T., Kumura-Ishii, K., Huang, J., Kodera, T., Ishii, T., Hirabayashi, Y., Koyanagi, Y., Sasaki, T., 2005. Ku80 autoantigen as a cellular coreceptor for human parvovirus B19 infection. Blood 106, 3449–3456.
Ozawa, K., Kurtzman, G., Young, N., 1987. Productive infection by B19 parvovirus of human erythroid bone marrow cells in vitro. Blood 70, 384–391.
Ozawa, K., Kurtzman, G., Young, N., 1986. Replication of the B19 parvovirus in human bone marrow cell cultures. Science 233, 883–886.
Pallier, C., Greco, A., Le Junter, J., Saib, A., Vassias, I., Morinet, F., 1997. The 3′ untranslated region of the B19 parvovirus capsid protein mRNAs inhibits its own mRNA translation in nonpermissive cells. J. Virol. 71, 9482–9489.
Pillet, S., Fichelson, S., Morinet, F., Young, N.S., Zhi, N., Wong, S., 2008. Human B19 erythrovirus in vitro replication: what's new? J. Virol. 82, 8951–8953.
Pillet, S., Le Guyader, N., Hofer, T., NguyenKhac, F., Koken, M., Aubin, J.T., Fichelson, S., Gassmann, M., Morinet, F., 2004. Hypoxia enhances human B19 erythrovirus gene expression in primary erythroid cells. Virology 327, 1–7.
Plevka, P., Hafenstein, S., Li, L., D'Abrgamo Jr., A., Cotmore, S.F., Rossmann, M.G., Tattersall, P., 2011. Structure of a packaging-defective mutant of minute virus of mice indicates that the genome is packaged via a pore at a 5-fold axis. J. Virol. 85, 4822–4827.
Ros, C., Gerber, M., Kempf, C., 2006. Conformational changes in the VP1-unique region of native human parvovirus B19 lead to exposure of internal sequences that play a role in virus neutralization and infectivity. J. Virol. 80, 12017–12024.
Servey, J.T., Reamy, B.V., Hodge, J., 2007. Clinical presentations of parvovirus B19 infection. Am. Fam. Physician 75, 373–376.
Shimomura, S., Komatsu, N., Frickhofen, N., Anderson, S., Kajigaya, S., Young, N.S., 1992. First continuous propagation of B19 parvovirus in a cell line. Blood 79, 18–24.
Takahashi, T., Ozawa, K., Takahashi, K., Asano, S., Takaku, F., 1990. Susceptibility of human erythropoietic cells to B19 parvovirus in vitro increases with differentiation. Blood 75, 603–610.
Timpe, J., Bevington, J., Casper, J., Dignam, J.D., Trempe, J.P., 2005. Mechanisms of adeno-associated virus genome encapsidation. Curr. Gene Ther. 5, 273–284.
Vihinen-Ranta, M., Wang, D., Weichert, W.S., Parrish, C.R., 2002. The VP1 N-terminal sequence of canine parvovirus affects nuclear transport of capsids and efficient cell infection. J. Virol. 76, 1884–1891.
Weigel-Kelley, K.A., Yoder, M.C., Srivastava, A., 2003. Alpha5beta1 integrin as a cellular coreceptor for human parvovirus B19: requirement of functional activation of beta1 integrin for viral entry. Blood 102, 3927–3933.
Wistuba, A., Kern, A., Weger, S., Grimm, D., Kleinschmidt, J.A., 1997. Subcellular compartmentalization of adeno-associated virus type 2 assembly. J. Virol. 71, 1341–1352.
Wong, S., Zhi, N., Filippone, C., Keyvanfar, K., Kajigaya, S., Brown, K.E., Young, N.S., 2008. Ex vivo-generated CD36+ erythroid progenitors are highly permissive to human parvovirus B19 replication. J. Virol. 82, 2470–2476.
Wong, S., Brown, K.E., 2006. Development of an improved method of detection of infectious parvovirus B19. J. Clin. Virol. 35, 407–413.
Zhi, N., Zádori, Z., Brown, K.E., Tijssen, P., 2004. Construction and sequencing of an infectious clone of the human parvovirus B19. Virology 318, 142–152.

Part III

Discussion

Bibliography

[1] P. Tijssen, Molecular and structural basis of the evolution of parvovirus tropism, *Acta Vet. Hung.* **47**, 379 (1999).

[2] A. M. Q. King, M. J. Adams, E. B. Carstens, and E. J. Lefkowitz, *Virus taxonomy: Ninth report of the International Committee on Taxonomy of Viruses.*, Elsevier Academic Press, San Diego, CA, 2012.

[3] C. Brailovsky, [Research on the rat K virus (Parvovirus ratti). I. A method of titration by plaques and its application to the study of the multiplication cycle of the virus], *Ann Inst Pasteur (Paris)* **110**, 49 (1966).

[4] J. R. Kerr, M. E. Bloom, S. Cotmore, R. M. Linden, and C. R. Parrish, *Parvoviruses*, Hodder Arnold, London, UK, 2005.

[5] V. V. Lukashov and J. Goudsmit, Evolutionary relationships among parvoviruses: virus-host coevolution among autonomous primate parvoviruses and links between adeno-associated and avian parvoviruses, *J. Virol.* **75**, 2729 (2001).

[6] M. E. Bloom, R. E. Race, and J. B. Wolfinbarger, Characterization of Aleutian disease virus as a parvovirus, *J. Virol.* **35**, 836 (1980).

[7] S. Alexandersen, M. E. Bloom, and S. Perryman, Detailed transcription map of Aleutian mink disease parvovirus, *J. Virol.* **62**, 3684 (1988).

[8] L. Li, P. A. Pesavento, L. Woods, D. L. Clifford, J. Luff, C. Wang, and E. Delwart, Novel amdovirus in gray foxes, *Emerging Infect. Dis.* **17**, 1876 (2011).

[9] R. McKenna, N. H. Olson, P. R. Chipman, T. S. Baker, T. F. Booth, J. Christensen, B. Aasted, J. M. Fox, M. E. Bloom, J. B. Wolfinbarger, and M. Agbandje-McKenna, Three-dimensional structure of Aleutian mink disease parvovirus: implications for disease pathogenicity, *J. Virol.* **73**, 6882 (1999).

[10] K. C. Chen, B. C. Shull, E. A. Moses, M. Lederman, E. R. Stout, and R. C. Bates, Complete nucleotide sequence and genome organization of bovine parvovirus, *J. Virol.* **60**, 1085 (1986).

[11] D. Schwartz, B. Green, L. E. Carmichael, and C. R. Parrish, The canine minute virus (minute virus of canines) is a distinct parvovirus that is most similar to bovine parvovirus, *Virology* **302**, 219 (2002).

[12] M. Lederman, J. T. Patton, E. R. Stout, and R. C. Bates, Virally coded noncapsid protein associated with bovine parvovirus infection, *J. Virol.* **49**, 315 (1984).

[13] K. I. Berns and S. Adler, Separation of two types of adeno-associated virus particles containing complementary polynucleotide chains, *J. Virol.* **9**, 394 (1972).

[14] J. A. Rose, K. I. Berns, M. D. Hoggan, and F. J. Koczot, Evidence for a single-stranded adenovirus-associated virus genome: formation of a DNA density hybrid on release of viral DNA, *Proc. Natl. Acad. Sci. U.S.A.* **64**, 863 (1969).

[15] E. Lusby, K. H. Fife, and K. I. Berns, Nucleotide sequence of the inverted terminal repetition in adeno-associated virus DNA, *J. Virol.* **34**, 402 (1980).

[16] M. R. Green and R. G. Roeder, Definition of a novel promoter for the major adenovirus-associated virus mRNA, *Cell* **22**, 231 (1980).

[17] E. W. Lusby and K. I. Berns, Mapping of the 5' termini of two adeno-associated virus 2 RNAs in the left half of the genome, *J. Virol.* **41**, 518 (1982).

[18] R. W. Atchison, The role of herpesviruses in adenovirus-associated virus replication in vitro, *Virology* **42**, 155 (1970).

[19] R. M. Buller, J. E. Janik, E. D. Sebring, and J. A. Rose, Herpes simplex virus types 1 and 2 completely help adenovirus-associated virus replication, *J. Virol.* **40**, 241 (1981).

[20] M. D. Hoggan, N. R. Blacklow, and W. P. Rowe, Studies of small DNA viruses found in various adenovirus preparations: physical, biological, and immunological characteristics, *Proc. Natl. Acad. Sci. U.S.A.* **55**, 1467 (1966).

[21] R. M. Kotin, M. Siniscalco, R. J. Samulski, X. D. Zhu, L. Hunter, C. A. Laughlin, S. McLaughlin, N. Muzyczka, M. Rocchi, and K. I. Berns, Site-specific integration by adeno-associated virus, *Proc. Natl. Acad. Sci. U.S.A.* **87**, 2211 (1990).

[22] R. M. Kotin, J. C. Menninger, D. C. Ward, and K. I. Berns, Mapping and direct visualization of a region-specific viral DNA integration site on chromosome 19q13-qter, *Genomics* **10**, 831 (1991).

[23] R. M. Kotin, R. M. Linden, and K. I. Berns, Characterization of a preferred site on human chromosome 19q for integration of adeno-associated virus DNA by non-homologous recombination, *EMBO J.* **11**, 5071 (1992).

[24] R. J. Samulski, X. Zhu, X. Xiao, J. D. Brook, D. E. Housman, N. Epstein, and L. A. Hunter, Targeted integration of adeno-associated virus (AAV) into human chromosome 19, *EMBO J.* **10**, 3941 (1991).

[25] V. Deiss, J. D. Tratschin, M. Weitz, and G. Siegl, Cloning of the human parvovirus B19 genome and structural analysis of its palindromic termini, *Virology* **175**, 247 (1990).

[26] C. Doerig, P. Beard, and B. Hirt, A transcriptional promoter of the human parvovirus B19 active in vitro and in vivo, *Virology* **157**, 539 (1987).

[27] K. Ozawa, J. Ayub, Y. S. Hao, G. Kurtzman, T. Shimada, and N. Young, Novel transcription map for the B19 (human) pathogenic parvovirus, *J. Virol.* **61**, 2395 (1987).

[28] E. D. Heegaard and K. E. Brown, Human parvovirus B19, *Clin. Microbiol. Rev.* **15**, 485 (2002).

[29] L. KILHAM and L. J. OLIVIER, A latent virus of rats isolated in tissue culture, *Virology* **7**, 428 (1959).

[30] R. C. Bates, C. E. Snyder, P. T. Banerjee, and S. Mitra, Autonomous parvovirus LuIII encapsidates equal amounts of plus and minus DNA strands, *J. Virol.* **49**, 319 (1984).

[31] C. R. Astell, M. Thomson, M. Merchlinsky, and D. C. Ward, The complete DNA sequence of minute virus of mice, an autonomous parvovirus, *Nucleic Acids Res.* **11**, 999 (1983).

[32] D. Pintel, D. Dadachanji, C. R. Astell, and D. C. Ward, The genome of minute virus of mice, an autonomous parvovirus, encodes two overlapping transcription units, *Nucleic Acids Res.* **11**, 1019 (1983).

[33] K. Hueffer and C. R. Parrish, Parvovirus host range, cell tropism and evolution, *Curr. Opin. Microbiol.* **6**, 392 (2003).

[34] L. V. Crawford, A minute virus of mice, *Virology* **29**, 605 (1966).

[35] G. D. Bonnard, E. K. Manders, D. A. Campbell, R. B. Herberman, and M. J. Collins, Immunosuppressive activity of a subline of the mouse EL-4 lymphoma. Evidence for minute virus of mice causing the inhibition, *J. Exp. Med.* **143**, 187 (1976).

[36] H. D. Engers, J. A. Louis, R. H. Zubler, and B. Hirt, Inhibition of T cell-mediated functions by MVM(i), a parvovirus closely related to minute virus of mice, *J. Immunol.* **127**, 2280 (1981).

[37] G. K. McMaster, P. Beard, H. D. Engers, and B. Hirt, Characterization of an immunosuppressive parvovirus related to the minute virus of mice, *J. Virol.* **38**, 317 (1981).

[38] D. G. Baker, Future Directions in Rodent Pathogen Control, *ILAR J* **39**, 312 (1998).

[39] E. M. Gardiner and P. Tattersall, Evidence that developmentally regulated control of gene expression by a parvoviral allotropic determinant is particle mediated, *J. Virol.* **62**, 1713 (1988).

[40] E. M. Gardiner and P. Tattersall, Mapping of the fibrotropic and lymphotropic host range determinants of the parvovirus minute virus of mice, *J. Virol.* **62**, 2605 (1988).

[41] J. P. Antonietti, R. Sahli, P. Beard, and B. Hirt, Characterization of the cell type-specific determinant in the genome of minute virus of mice, *J. Virol.* **62** (1988).

[42] M. Agbandje-McKenna, A. L. Llamas-Saiz, F. Wang, P. Tattersall, and M. G. Rossmann, Functional implications of the structure of the murine parvovirus, minute virus of mice, *Structure* **6**, 1369 (1998).

[43] M. E. Bloom, B. D. Berry, W. Wei, S. Perryman, and J. B. Wolfinbarger, Characterization of chimeric full-length molecular clones of Aleutian mink disease parvovirus (ADV): identification of a determinant governing replication of ADV in cell culture, *J. Virol.* **67**, 5976 (1993).

[44] J. Bergeron, B. Hebert, and P. Tijssen, Genome organization of the Kresse strain of porcine parvovirus: identification of the allotropic determinant and comparison with those of NADL-2 and field isolates, *J. Virol.* **70**, 2508 (1996).

[45] C. R. Parrish, C. F. Aquadro, and L. E. Carmichael, Canine host range and a specific epitope map along with variant sequences in the capsid protein gene of canine parvovirus and related feline, mink, and raccoon parvoviruses, *Virology* **166**, 293 (1988).

[46] S. F. Chang, J. Y. Sgro, and C. R. Parrish, Multiple amino acids in the capsid structure of canine parvovirus coordinately determine the canine host range and specific antigenic and hemagglutination properties, *J. Virol.* **66**, 6858 (1992).

[47] U. Truyen, M. Agbandje, and C. R. Parrish, Characterization of the feline host range and a specific epitope of feline panleukopenia virus, *Virology* **200**, 494 (1994).

[48] C. Ros, C. Baltzer, B. Mani, and C. Kempf, Parvovirus uncoating in vitro reveals a mechanism of DNA release without capsid disassembly and striking differences in encapsidated DNA stability, *Virology* **345**, 137 (2006).

[49] M. Agbandje, C. Parrish, and M. Rossmann, The structure of parvoviruses, *Seminars in Virology* **6**, 299 (1995).

[50] M. Agbandje, R. McKenna, M. G. Rossmann, M. L. Strassheim, and C. R. Parrish, Structure determination of feline panleukopenia virus empty particles, *Proteins* **16**, 155 (1993).

[51] A. A. Simpson, B. Hebert, G. M. Sullivan, C. R. Parrish, Z. Zadori, P. Tijssen, and M. G. Rossmann, The structure of porcine parvovirus: comparison with related viruses, *J. Mol. Biol.* **315**, 1189 (2002).

[52] J. Tsao, M. S. Chapman, M. Agbandje, W. Keller, K. Smith, H. Wu, M. Luo, T. J. Smith, M. G. Rossmann, and R. W. Compans, The three-dimensional structure of canine parvovirus and its functional implications, *Science* **251**, 1456 (1991).

[53] A. L. Llamas-Saiz, M. Agbandje-McKenna, W. R. Wikoff, J. Bratton, P. Tattersall, and M. G. Rossmann, Structure determination of minute virus of mice, *Acta Crystallogr. D Biol. Crystallogr.* **53**, 93 (1997).

[54] M. G. Rossmann and J. E. Johnson, Icosahedral RNA virus structure, *Annu. Rev. Biochem.* **58**, 533 (1989).

[55] H. Wu, W. Keller, and M. G. Rossmann, Determination and refinement of the canine parvovirus empty-capsid structure, *Acta Crystallogr. D Biol. Crystallogr.* **49**, 572 (1993).

[56] Q. Xie and M. S. Chapman, Canine parvovirus capsid structure, analyzed at 2.9 A resolution, *J. Mol. Biol.* **264**, 497 (1996).

[57] M. S. Chapman and M. G. Rossmann, Structure, sequence, and function correlations among parvoviruses, *Virology* **194**, 491 (1993).

[58] M. S. Chapman and M. G. Rossmann, Single-stranded DNA-protein interactions in canine parvovirus, *Structure* **3**, 151 (1995).

[59] J. Tsao, M. S. Chapman, H. Wu, M. Agbandje, W. Keller, and M. G. Rossmann, Structure determination of monoclinic canine parvovirus, *Acta Crystallogr., B* **48 (Pt 1)**, 75 (1992).

[60] J. W. LITTLEFIELD, THREE DEGREES OF GUANYLIC ACID–INOSINIC ACID PYROPHOSPHORYLASE DEFICIENCY IN MOUSE FIBROBLASTS, *Nature* **203**, 1142 (1964).

[61] H. M. SHEIN and J. F. ENDERS, Multiplication and cytopathogenicity of Simian vacuolating virus 40 in cultures of human tissues, *Proc. Soc. Exp. Biol. Med.* **109**, 495 (1962).

[62] E. Harlow, L. V. Crawford, D. C. Pim, and N. M. Williamson, Monoclonal antibodies specific for simian virus 40 tumor antigens, *J. Virol.* **39**, 861 (1981).